ADVANCED TECHNOLOGY LABORATORIES

65 p.

DESIGN CRITERIA FOR ZERO-LEAKAGE CONNECTORS FOR LAUNCH VEHICLES. VOL. 1, SUMMARY, CONCLUSIONS, AND DESIGN EXAMPLES

Edited by
T.P. GOODMAN

CONTRACT NAS 8-4012

MARCH 15, 1963

GENERAL ELECTRIC

INTERIM
~~FINAL~~ REPORT FOR FIRST CONTRACT PERIOD

(March 1962 through February 1963)

DESIGN CRITERIA FOR ZERO-LEAKAGE CONNECTORS FOR LAUNCH VEHICLES

Contract NAS 8-4012

VOLUME 1

SUMMARY, CONCLUSIONS, AND DESIGN EXAMPLES

Edited by T.P. Goodman

March 15, 1963

PREPARED FOR: Propulsion and Vehicle Engineering Division
George C. Marshall Space Flight Center
National Aeronautics and Space Administration
Huntsville, Alabama

PREPARED BY: Advanced Technology Laboratories
General Electric Company
Schenectady, New York

SPONSORED BY: Missile and Space Division
General Electric Company
Philadelphia, Pennsylvania

N.A.S.A. TECHNICAL MANAGER: C.C. Wood (M-P&VE-PT)

CONTENTS

11. PROJECT SCOPE

by

T.P. Goodman

18390

11.0 Summary

The goal of this investigation is "to establish the fundamental design criteria that will provide for zero leakage in separable connectors used in launch vehicles."

The approach taken in the investigation has been to regard a separable connector as an interface between two surfaces, backed up by a supporting structure, designed to withstand a variety of environmental conditions. The project has included both analytical and experimental investigation of the sealing action at the seal interface, together with analytical investigation of the supporting structure and the environmental conditions to which a launch vehicle is subject. The application of design criteria is illustrated by three representative design examples.

The principal conclusions from this investigation are:

1. Substantial plastic flow of at least one of the materials at the seal interface is necessary for zero leakage.

2. The plastic flow required for zero leakage can never be achieved in a conventional flared fitting with metal-to-metal contact, because the fitting will fail by hoop compression before the plastic stress range is reached at the seal interface.

3. To reduce the effect of flange rolling in the larger sizes of bolted flanged connectors, efficient lightweight designs can often be obtained by having the flanges in contact outside the bolt circle.

4. The many interacting factors in connector design can best be evaluated by building and testing connectors for specific applications.

During the second contract period (March 1963 to November 1963) we are following up on Conclusion No. 4 by designing, building, and testing connectors for three specific applications.

11.1 Project Goal

For the first contract period (March 1962 to February 1963) covered by this report, the goal of the project, as expressed in the Work Statement provided by NASA, has been "to establish the fundamental design criteria that will provide for zero leakage in separable connectors used in launch vehicles."

This report discusses the design criteria that were considered in the course of the study. The purpose of the report is to provide this information in sufficient detail so that it can be applied in the design of connectors for improved zero-leakage performance.

The specific topics mentioned in the Work Statement provided by NASA are listed below, with the principal sections of this report in which they are discussed indicated in parentheses.

1. Surface finish (Sections 31-37)
2. Flow through capillaries (Section 22)
3. Number of flow paths (minimize) (Sections 22, 36)
4. Threshold pressure for zero leakage (Sections 21, 36)
5. Load (Section 40)
6. Asymmetrical loading and installation (Section 47)
7. Warpage (Section 46)
8. Fatigue (Section 40)
9. Setting of materials (especially seals) (Section 45)
10. Transient temperature (Section 61)
11. Thermal shock (Section 61)
12. Water-hammer effect (Section 62)
13. Vibration (Section 63)
14. Handling (Section 63)

Additional problem areas discussed in the first quarterly review meeting were as follows:

15. Vacuum environment (Section 64)
16. Radiation environment (Section 64)

The interrelationships among these various problem areas are illustrated by the three design examples presented in Section 13.

11.2 Approach Taken in Project

The problem of establishing design criteria for zero-leakage connectors has been approached in this investigation by regarding a separable fluid connector as an interface between two surfaces backed up by a supporting structure designed to withstand a variety of environmental conditions. This approach made it possible to divide the investigation into three separate but related parts.

The sealing action at the seal interface has been investigated both analytically and experimentally. The analytical investigation (Sections 32 and 33) indicated the expected trend of the results, but experiments were needed because of the many uncertain assumptions in the analysis. The experiments included metallic, plastic, and elastomeric gasket materials in contact with stainless-steel and aluminum test flanges. To eliminate the uncertainties of bolt friction, the compressive sealing load was applied by a universal testing machine. To provide quantitative measurements of leakage in the "zero-leakage" range, the joints were pressurized with helium and the leakage flow was measured with a mass-spectrometer leak detector. Surface finishes before and after sealing were recorded with a "Talysurf" profile recorder and a Zeiss interference microscope. To aid in interpreting the results, the leakage flow was calculated both for typical flow passages at seal interfaces and for permeation flow through metallic, plastic, and elastomeric materials.

The supporting structure was analyzed as a combination of flange, gasket, and pipe. Since the stresses in flange and pipe are intended to remain in the elastic range, where calculations give reliable results, this part of the investigation was done by analysis. Design procedures were worked out for flange joints both with and without contact outside the bolt circle, the goal being an efficient design in which all parts of the joint are equally stressed. The effect of bolt spacing, thermal contraction at low temperatures, creep at high temperatures, warping, bending and misalignment, and thermal distortion was analyzed. A separate analysis was made for flared fittings. Pressure-energized seals of both the cantilever type and the metallic O-ring type were analyzed and compared.

In the consideration of environmental effects, emphasis was on the corrections required to static analysis, or on the equivalent additional static loading, to represent the environmental effect. Thus the analysis of thermal transients was designed to show how the temperature distribution in a flange can be determined, to make possible the calculation of thermal stresses and deformations. The effect of pressure surges (water hammer) was studied to determine what maximum surge pressure should be used in design and what could be done to reduce this surge pressure. The goal of the analysis of shock and vibration on connector systems was to show how the shock and vibration load on the connector system can be represented by equivalent additional static or low-cycle loads on the connector itself. The goal of the review of environmental effects on polymeric gasket materials is to determine what design values of mechanical properties such as stress and elastic modulus should be used in extreme environmental conditions.

11.3 Principal Conclusions

While the conclusions from the various parts of this study are given in each section of the report, it may be useful to list some principal conclusions emerging from the study that appear to have the greatest significance for zero-leakage fluid-connector design. The four conclusions discussed below may be designated as principal conclusions from this study.

1. Substantial plastic flow of at least one of the materials at the seal interface is necessary for zero leakage. This conclusion follows from the leakage-flow tests of Section 36, supporting the qualitative conclusions from the analysis of Section 33. For metallic gasket materials, this means that the stress must be above the yield stress -- preferably about twice the yield stress for essentially complete sealing. In addition, the gasket material must have an opportunity to flow; if it is contained so that the sealing stress builds up hydrostatic pressure rather than shear deformation, sealing will not occur. For plastic gasket materials, much lower stresses are possible, due to the viscoelastic nature of these materials; the viscoelastic phase of such a material flows and seals the leak before the yield stress of the elastic phase is reached. For elastomeric gasket materials, extremely low stresses are possible for sealing. Material compatibility problems and environment problems pose the principal limitations on the application of elastomers as seals.

While we have not yet tested gasketless joints with metal-to-metal contact, it appears that they will be extremely difficult to seal with zero leakage unless the stress can be localized. Otherwise the parts will fail by gross deformation before adequate stresses for sealing have been attained.

2. The plastic flow required for zero leakage can never be achieved in a conventional flared fitting with metal-to-metal contact, because the fitting will fail by hoop compression before the plastic stress range is reached at the seal interface. This conclusion, discussed in detail in Section 49, follows from Conclusion No. 1. At the interface between the flare fitting and the flared tube, the hoop compressive stress is necessarily greater than the normal sealing stress, because the cross-sectional area over which the hoop compressive stress acts is less than the area of the normal sealing surface. Consequently, before the stress at the seal interface can reach twice the yield stress, the fitting will have already failed by hoop compression.

This reasoning suggests that flared fittings should be redesigned in one of the following ways:

(a) Sealing surfaces should be of a more yieldable material than the connector parts that apply the sealing stress

(b) Sealing stress should be localized

(c) The flare elements with obliquely applied sealing stress should be replaced by elements in which the sealing stress is applied axially.

3. To reduce the effect of flange rolling in the larger sizes of bolted flanged connectors, efficient lightweight designs can often be obtained by having the flanges in contact outside the bolt circle. In elementary approaches to the design of flanged connectors, it is customary to consider the stretch of the bolts and the compression of the gasket, but to neglect the rolling of the flanges as the bolts are tightened. This simplification is valid if the flanges are massive and rigid, but in lightweight designs -- which are of the greatest interest for missile applications -- the rolling of the flanges is an elastic deformation that must be considered along with the deformations of bolts and gaskets. In cryogenic connectors (Section 44), flange rolling may be beneficial in providing elastic springback to maintain compressive stress on a gasket in spite of thermal contraction. However, in other designs, flange rolling can cause the sealing stress on the gasket to decrease as the bolts are tightened! To reduce the amount of flange rolling, and hence to achieve an efficient lightweight connector design, the flanges may be designed to contact outside the bolt circle, as described in Section 41. By contrast, an unsatisfactory design in which the flanges are not in contact outside the bolt circle is discussed in the design example of Section 13.1. This discussion explains analytically the observed failure of a connector during tests in Huntsville due to rolling of the flange and barreling of the pipe.

4. The many interacting factors in connector design can best be evaluated by building and testing connectors for specific applications. This complexity of the stresses in a flange or flare connector, as illustrated by the analyses of Volume 4, precludes the possibility of designing connectors by any short list of simple design rules. The application of the various design criteria requires design judgement and design compromises at many stages of the design process. We feel that these design criteria can best be validated and appreciated by experience. To provide this experience, we plan, during the second contract period, to apply these criteria to the design of representative connectors that will be built and tested.

8

11.4 Suggestions for Future Investigations

As a result of the present study, several areas have emerged that appear to deserve further investigation. Items 1, 5 and 6 below are included in our program for the Second Contract Period, as indicated in Section 11.5. Item 3 below is included in the program for the second contract period of Contract NAS 7-102, "Study of Dynamic and Static Seals for Liquid Rocket Engines."

1. Further experiments are needed on the phenomenon of sealing action to supplement the results reported in Volume 3 of this report for metal-to-gasket mating of flat surfaces. These experiments can be performed with the apparatus that is already available.

   a. The mating of two flat metal surfaces of the same material should be investigated. Such tests would represent the metal-to-metal mating that occurs in conventional flared fittings and other gasketless joints.

   b. Other geometries such as curved surfaces and knife-edge surfaces, which give promise of providing more highly localized sealing stress, should be tested. Then the geometries that show the greatest promise in these tests can be incorporated in improved connector designs.

2. The effect of relative sliding motion of surfaces on sealing effectiveness should be investigated. This effect is important in connectors where the seal is effected at room temperature and where the joint is expected to be leak-tight at cryogenic or pyrogenic temperatures, after relative thermal contraction or expansion has taken place. We want to find out whether such a joint can re-seal after sliding motion has taken place, or whether sliding must be prevented to achieve reliable sealing.

3. A study should be made of the various methods of leak detection and the types of leakage flow that occur in the leak paths of fluid connectors. From such a study, recommendations could be made for the most suitable leak-monitoring device for a given connector. Also, an understanding of the types of flow occurring in the leak paths should make it possible to predict the leakage that would occur at high pressure with a given fluid from measurements made at lower pressures and with other fluids.

4. An effort should be made to develop LOX-compatible materials for use as low-temperature seals. At present, all the elastomeric materials that are most effective in sealing at low temperatures, as shown by tests performed at the National Bureau of Standards, are LOX-sensitive and therefore unsuitable for sealing LOX lines (see Section 44.1).

5. The design criteria developed in this study should be verified by building and testing representative connectors for specific applications.

6. On the basis of the tests of these representative connectors, a Handbook of Proven Connector Design Principles should be prepared.

11.5 Plans for Second Contract Period

During the second contract period (March 1963 to November 1963) we plan to prove out the connector design criteria developed in the first contract period and described in this report, by designing, fabricating, and testing representative fluid connectors for typical applications. The plan for the second contract period is as follows:

I. Continuing experimental investigation of effect of gasket material properties and geometry on leakage flow. This task will include continuation of experimental tests to determine the relationship among surface finish, sealing pressure, internal pressure, and leakage for promising gasket materials, including some of the gasket materials being developed under another NASA contract. In addition to flat mating surfaces, we plan to test some examples of other geometries such as flat surfaces vs. curved surfaces and flat surfaces vs. knife-edge surfaces.

II. Design of improved connectors employing design criteria of first-year program.

A. Tube connectors for high-pressure gases (using various techniques for obtaining adequate sealing pressure without overstressing connector parts).

B. Flange connectors for low-temperature liquid-oxygen and liquid-hydrogen service (using various principles of pressure self-energizing and temperature compensation).

C. Flange connectors for high-temperature, high-pressure service.

III. Fabrication and assembly of improved connectors designed in Part II.

IV. "Proof-of-principle" testing of improved connectors designed in Part II. These tests will be conducted in Schenectady under simulated service conditions. They will duplicate the internal pressures and static loading conditions to which connectors are subjected in service. Preliminary testing will be done at room temperature, using gasket materials whose room-temperature behavior simulates the high-temperature and low-temperature behavior of actual gasket materials. Additional testing will be done at operating temperatures, using liquid nitrogen in place of liquid oxygen. The effect of shock and vibration on the connector system will be represented for leakage tests by static and low-cycle loading on the connector itself. These tests will be primarily intended to measure leakage to determine the effectiveness of the connector designs. Stress and deflection measurements will also be made to verify the intermediate steps in the design calculations.

V. Analysis of results and preparation of a Handbook of Proven Connector Design Principles (final project report)

A. Analysis of results, including correlation of design calculations with test results and revision of design methods as required. In connection with this phase of the work, close liaison will be maintained with the Air Force contracts at Armour Research Foundation and Battelle Memorial Institute, and with any pertinent test programs in Huntsville and other programs as they apply.

B. Publication of a Handbook of Proven Connector Design Principles (final project report with interim monthly and quarterly reports as required by the Contract.

12. ORGANIZATION OF REPORT

by
T.P. Goodman

Reflecting the approach taken in this investigation, the present report has been divided into six volumes, as follows:

Volume 1. Summary, Conclusions, Design Examples
(Sections 11 through 13)

Volume 2. Leakage Flow
(Sections 21 through 24)

Volume 3. Sealing Action at the Seal Interface
(Sections 31 through 37)

Volume 4. Design of Connectors
(Sections 40 through 49)

Volume 5. Pressure-Energized Seals
(Sections 51 through 53)

Volume 6. Environmental Effects
(Sections 61 through 64)

The two-digit numbering system for sections of the report was adopted to facilitate reference to the separate volumes.

The contents of the individual volumes and sections and the relationships among them are indicated briefly in this section. In addition, a summary of each section will be found at the beginning of that section. In many sections, particularly in Volume 4, the conclusions that would be of general interest are discussed in the earlier sub-sections, while the detailed mathematical derivations are included in later sub-sections as appendices. The last sub-section of each section is a list of references.

Volume 1 is devoted to general matters and includes a summary of the project itself (Section 11), a summary of this report (Section 12), and a group of three design examples (Section 13). The examples considered are two floating-ring flange joints - one with a metallic O-ring seal and one with a modified MC fitting with metal-to-metal contact - and a "Naflex" cantilever-type pressure-energized seal with flanges contacting outside the bolt circle. The deformations and stresses in these connectors are analyzed, and recommendations are made for design changes for improved performance. In both connectors using floating-ring flanges, performance could be improved by allowing the rings to contact outside the bolt circle.

Volume 2 considers the analysis and measurement of leakage flow. Section 21 describes the two regimes of flow - laminar (viscous) flow and molecular diffusion flow - that are involved in the leakage phenomenon and discusses the means that can be used to measure flows in the "zero-leakage" range. Section 22 presents formulas for calculating the leakage flow through small passages, in both the laminar-flow and molecular-flow regimes. Graphs are included to give leakage flow as a function of pressure and clearance for a leakage-flow passage of typical dimensions, and formulas are included for converting to flows for other dimensions and conditions. The leakage at a joint must always be considered in relation to the leakage that would occur by permeation through a solid pipe or a solid gasket material; the permeation phenomenon is discussed in Section 23, giving experimental results for the flange and gasket materials that are of greatest interest, together with formulas for taking into consideration the effects of temperature and pressure. Since most flanged connectors are joined to pipes by welded, brazed, or soldered joints and since these types of joints provide an alternative to separable connectors in many applications, Section 24 briefly reviews these metal-joining processes. This section also discusses some of the precautions and inspection methods that should be applied to assure that a joint made by these metal-joining processes will have the same leak-tightness as a continuous solid pipe.

Volume 3 reports the analytical and experimental investigation of the interaction of gasket and flange at the seal interface. Section 31 describes the goals of this investigation and the resulting conclusions and recommendations. Section 32 is an analysis of the elastic and plastic action between a hard, smooth metal flange and a soft, machined metal gasket, explaining the regimes of surface mating encountered in the experiments. Section 33 is an analysis, based on plastic flow and a statistical model of surface roughness, of the mating of microscopic asperities and the resulting sealing of microscopic flow passages. Section 34 describes the mechanical properties of the stainless-steel and aluminum flange materials and the metallic, plastic, and elastomeric gasket materials used in the tests; the permeation data of Section 23 are supplemented by additional permeation data for the plastic and elastomeric gasket materials to compare leakage rates with permeation rates. Section 35 describes the testing procedure for measuring leakage flow as a function of internal fluid pressure and compressive sealing stress, as well as the surface-profile and interference-microscope inspection of surface finishes before and after compression. Section 36 presents the results of the experiments described in Section 35. Section 37 includes a discussion of these results and a comparison with analytical predictions, along with the conclusions from this phase of the investigation. The basic conclusion from Volume 3 is that substantial plastic flow of the softer mating material is needed for zero leakage; with plastic or elastomeric gasket material having viscoelastic properties, the required plastic flow of the viscoelastic phase of the material can be achieved at pressures well below the yield point of the elastic phase, as determined from tensile or compressive tests.

Volume 4 analyzes the design of the supporting structure needed to supply the required compressive sealing force at the seal interface. Since the supporting structure is intended to stay in the stress range below the yield point, calculations based on experimentally-determined material properties are used for the stress determination. The design procedures described in Volume 4 will be verified by applying them to specific connector designs that will be built and tested during the second contract period. Section 40 reviews

briefly the interaction of flange, gasket, and pipe and the various factors that enter into a connector design. Sections 41 and 42 present procedures for designing flanged connectors with and without contact of the flanges outside the bolt circle; by carrying out the design both ways, it can be determined which design procedure leads to a more efficient use of material - hence to a lighter weight - in a given application. Section 43 presents an analysis of the contact pressure due to bolt spacing and suggests that to achieve the most nearly uniform clamping, the bolts should be placed as close together as wrench clearance permits.

Sections 44 and 45 consider the special problems of low-temperature and high-temperature flange connector design. Section 44 considers the problems of the thermal contractions of parts and the hardening of gasket materials at low temperatures, and suggests the exploitation of differential thermal expansion - such as by using aluminum bolts in steel flanges or by using invar rings - to maintain leaktightness as the joint cools down. Section 45 considers the effect of creep at high temperatures, and a design example shows that the bolts may creep more than the gasket.

Sections 46 and 47 consider the effects of warping, external bending moment and misalignment on flange assemblies. The analysis shows that the bolt loads necessary to overcome these effects and provide uniform gasket compression may be substantial and should always be considered.

Section 48 analyzes the thermal distortion of flanges and develops a simplified procedure for calculating this effect.

Section 49 analyzes the stresses in flare-type demountable tubing connectors. It is concluded that a conventional flared fitting with metal-to-metal contact can never achieve zero leakage, because the fitting will fail by hoop compression before the stress at the seal interface can become sufficient for sealing.

Pressure-energized seals offer atractive possibilities for sealing against high pressures. With a conventional flat gasket, the sealing pressure decreases with increasing fluid pressure, but by using a pressure-energized seal, the sealing pressure can be made to increase with increasing fluid pressure. Volume 5 considers the design of two types of seals with a pressure-energizing effect. Section 51 discusses cantilever-type seals, known under the trade names of "Naflex," "Pneuflex," and "K-seals." Section 52 discusses hollow metallic O-rings and shows that the standard O-rings, as well as the "pressure-energized" and "pressure-filled" types, have a pressure-energizing action. Section 53 is a comparison between the two types of seals.

Environmental conditions to which fluid connectors in launch vehicles may be subjected are considered in Volume 6. Section 61 discusses temperature transients. Data on heat-transfer coefficients are presented, and it is shown how a simplified analytical approach can yield information on transient temperature distributions that would be sufficient for the calculation of stresses and leakage. Section 62 discusses the water-hammer effect and shows how to compute the maximum surge pressure, as well as suggesting how it can be reduced. Section 63 shows how shock and vibration loads on a connector system affect the loading on the connector itself. It is concluded that the effect of shock and vibration on the connector system can be represented by an

additional static or low-cycle bending load on the connector itself. In typical examples, it is found that the bending loads attained are substantial in comparison with other loads on the connector. Section 64 shows the effects of vacuum, radiation, and temperature environments on polymeric gasket materials. It appears that for most environments encountered by launch vehicles, the vacuum and radiation effects will not be a problem. However, thermal degradation and creep at high temperatures and the substantial increase in modulus of elasticity at low temperatures, below the glass transition temperature, must be considered in connector design.

This report includes the material previously reported in the three Quarterly Progress Reports issued for this project. Thus this report is self-contained without reference to the Quarterly Progress Reports.

13. DESIGN EXAMPLES

by

B.T. Fang, C.H. Gay, S. Levy, and J. Wallach

13.0 Summary

Analyses are presented for three typical connectors. One uses an O-ring seal (Sec. 13.1), another uses a Naflex seal (Sec. 13.2), and the third makes metal-to-metal contact (Sec. 13.3). Both aluminum and steel are considered as flange and bolt materials.

The analyses show that deformations due to initial bolting, pressure, and temperature are substantial. Major sources of uncertainty in the analyses arise from frictional effects and from lack of knowledge regarding the confined yielding of sealing materials such as teflon. Nevertheless it is shown that each connector will leak under certain circumstances.

Where indicated by the analysis, recommendations are given for the improvement of the connectors. In both connectors using floating ring flanges (Secs. 13.1 and 13.3), the rolling of the ring is substantial. Contact for these rings outside the bolt circle would stiffen them and improve their performance.

15

13.1 Flange Joint with Metallic O-ring Seal (by B.T. Fang)

13.1.1 Description of the Joint

A test connector is shown in Huntsville drawing SK 20-1286. An aluminum (6061 T6) tube of 0.125 in. wall thickness is joined to a steel (CRES 321) tube of 0.093 in. wall thickness. Both tubes have the same inside diameter of 20.250 in. Welded to the aluminum tube is a flange of the same material. On the steel tube side a loose aluminum (7075 T6) flange is used which is slipped on a ferrule welded to the steel tube. In between the lip of the ferrule and the integral flange is a spacer of $0.145 \begin{smallmatrix} + 0.005 \\ - 0.000 \end{smallmatrix}$ in. thickness and made of CRES 321 steel. The spacer serves as a retaining ring and also limits the compression of the gasket which is a U-2632-21250-NPE metallic O-ring. Forty bolts are used which are made of high-strength alloy steel. The connector is subjected to the following loading and temperature environment:

(1) Prior to flight pressure, there are

(a) Axial compression of 25,000 lb.

(b) Shear of 27,000 lb.

(c) Moment of 354,000 in-lb.

(2) Operating pressure of 185 psi. Proof pressure of 1.5 times the operating pressure.

(3) Temperature of -290°F, chilled at negligible pressure.

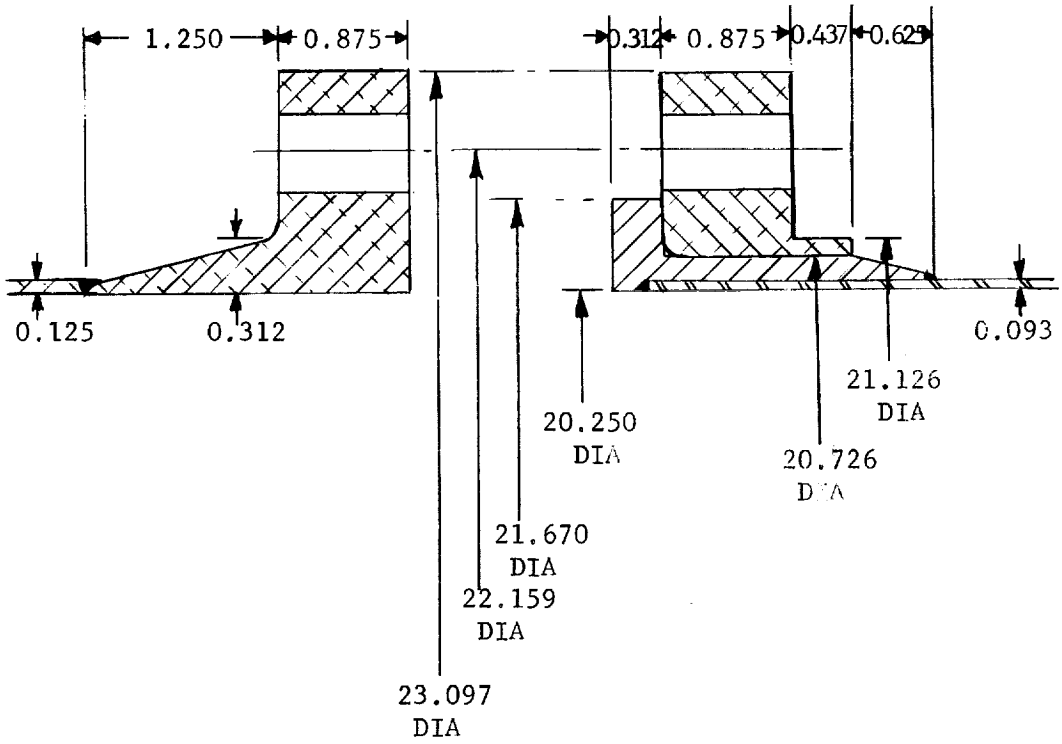

FIGURE 13.1 Huntsville Drawing SK20-1286

13.1.2 Determination of Compliances of Connector Components

In order to determine the behavior of the connector it is convenient to calculate first the compliances of the individual components. By compliance we mean the characteristic quantity which when multiplied by the force, moment and temperature, gives the corresponding deflection, rotation, etc.

A. Bolts

(a) Elastic Compliance

$$q_B = \frac{\text{effective length}}{(\text{Young's modulus})(\text{total bolt area})}$$

$$= \frac{2.438}{(30\times10^6)\ (40 \times 0.1060)} \qquad (1)$$

$$= 1.92 \times 10^{-8} \text{ in/lb.}$$

(b) Thermal Compliance

$$k_B = (\text{effective length})(\text{coefficient of thermal expansion})$$

$$= (2.2)(6 \times 10^{-6}) \qquad (2)$$

$$= 1.32 \times 10^{-5} \text{ in/}^{o}\text{F}$$

B. Gasket (O-ring)

(a) Elastic Compliance

From Section 52 we have

$$q_G = \frac{b^3 \left[0.149 - 0.141/(1+14.4/\mu^2)\right]}{D} \Big/ (\pi)\ (21.250)$$

$$= \frac{\left(\frac{3}{32}\right)^3 \left\{0.149 - 0.141/\left[1+(14.4)(10.125)(0.032)/(12)(0.91)\left(\frac{3}{32}\right)^2\right]\right\}}{(30 \times 10^6)(0.032)^3\ (12 \times 0.91)(\pi)(21.250)}$$

$$= 1.98 \times 10^{-8} \text{ in/lb.} \qquad (3)$$

C. Spacer

(a) Elastic Compliance

$$q_S = \frac{(\text{thickness})}{(\text{Young's modulus})(\text{total spacer area})}$$

$$= \frac{0.145}{(30\times10^{6})(\pi)(21.47)(0.2)} \qquad (4a)$$

$$= 3.58 \times 10^{-10} \text{ in/lb.}$$

Sometimes we have to consider the ferrule lip as a part of the spacer. In that case the elastic compliance of the spacer and ferrule lip combined is

$$q_S + q_f = q_s \left(1 + \frac{\text{ferrule lip thickness}}{\text{spacer thickness}}\right)$$

$$= 3.58 \times 10^{-10} \left(1 + \frac{0.312}{0.145}\right) \qquad (4b)$$

$$= 1.13 \times 10^{-9} \text{ in/lb}$$

(b) Thermal Compliance (axial)

$$K_{sa} = (\text{thickness})(\text{coefficient of thermal expansion})$$

$$= (0.145)(9.2\times10^{-6}) \qquad (5)$$

$$= 1.33 \times 10^{-6} \text{ in/}^{o}\text{F}$$

(c) Thermal Compliance (radial)

$$K_{sr} = (\text{mean diameter})(\text{coefficient of thermal expansion})$$

$$= (21.47)\ (9.2 \times 10^{-6}) \qquad (6)$$

$$= 1.98 \times 10^{-4} \text{ in/}^{o}\text{F}$$

D. Integral Flange

(a) Elastic compliance (moment-rotation)

From Ref. 1 we have

$$q_{FM} = \frac{(1-\mu^2)\ V}{L\ h_o g_o^{\ 2}\ E_F}$$

where E_F is Young's modulus, μ is Poisson's ratio, h_o and g_o are characteristic dimensions of the flange. V and L can be determined from the curves given in ASME Code (Ref. 2). For the present flange

V = 0.128

L = 0.956

Therefore

$$q_{FM} = \frac{(0.891)\ (0.128)}{0.956\ \sqrt{(20.25)(0.125)}\ (0.125)^2\ (10 \times 10^6)} \qquad (7)$$

$$= 4.81 \times 10^{-7} \text{ rad/lb-in}$$

(b) Elastic Compliance (internal pressure-rotation due to barreling effect)

From Ref. 3 we have

$$q_{FA} \cong \frac{c_1\ B^2\ \gamma}{t\ (t^2 + c_2\ g_e\ \gamma)}$$

where $c_1 = \frac{\sqrt{3}\ (2-\mu)}{4\ E_F\ \sqrt{(1-\mu^2)}} = \frac{\sqrt{3}\ (2-0.33)}{4\ (10 \times 10^6)\ \sqrt{1-0.33^2}} = 7.66 \times 10^{-8}$

$$c_2 = \sqrt{\frac{3}{1-\mu^2}} = \sqrt{\frac{3}{1-0.33^2}} = 1.84$$

t = flange thickness = 0.875

$$\gamma = \frac{g_e\ (\mu+Z)\left(1 + \frac{c_3 t}{h_o}\right)}{1 + \frac{(c_4 B\ g_e^3\ (\mu+Z)}{h_o t^3}\quad (2 + \frac{c_3 t}{h_o})}$$

$$c_3 = \sqrt[4]{12\ (1-0.33^2)} = 1.81$$

$$c_4 = \frac{c_3}{2\ (1-0.33^2)} = 1.02$$

g_e = weighted average thickness of hub = 0.21

Z = 8 as determined from the curve in ASME Code

Therefore

$$\gamma = \frac{0.21\ (0.33+8)\left(1 + \frac{(1.81)(0.875)}{0.21}\right)}{1 + \frac{(1.02)(20.25)(0.21)^3(0.33+8)}{\sqrt{(20.25)(0.125)}\ (0.875)^3}\quad (2 + \frac{(1.81)(0.875)}{0.21})}$$

$$= \frac{(0.21)(8.33)(8.55)}{1 + (1.49)(9.55)}$$

$$= 0.985$$

And

$$q_{Fp} = \frac{7.66 \times 10^{-8} \ (20.25)^2 \ (0.985)}{(0.875) \left[(0.875)^2 + (1.84)(0.21)(0.985)\right]} \qquad (8)$$

$$= 3.07 \times 10^{-5} \text{ rad/psi}$$

(c) Thermal Compliance (axial)

$$K_{Fa} = \text{(flange thickness)(coefficient of thermal expansion)}$$

$$= (0.875) \ (12 \times 10^{-6}) \qquad (9)$$

$$= 1.05 \times 10^{-5} \text{ in/}^{o}\text{F}$$

(d) Thermal Compliance (radial)

$$K_{Fr} = \text{(mean diameter)(coefficient of thermal expansion)}$$

$$= (21.67) \ (12 \times 10^{-6}) \qquad (10)$$

$$= 2.60 \times 10^{-4} \text{ in/}^{o}\text{F}$$

E. Loose Flange

(a) Elastic Compliance

$$q'_{FM} = \frac{(1-\mu^2) \ V}{L \ h_o \ g_o^{\ 2} \ E_F}$$

For the present loose flange it can be determined from the curves given in ASME Code that

$$V = 15$$

$$L = 9.13$$

Therefore

$$q'_{FM} = \frac{(0.891)\ (15)}{(9.13)\ \sqrt{(20.25)(0.2)}\ \ (0.2)^2\ (10\text{x}10^6)} \qquad (11)$$

$$= 1.82 \times 10^{-6} \text{ rad/lb-in.}$$

(b) Thermal Compliance (axial)

$$K'_{Fa} = 1.05 \times 10^{-5} \text{ in/}^{o}\text{F} \qquad (12)$$

(c) Thermal Compliance (radial)

$$K'_{Fr} = (21.91)\ (12\text{x}10^{-6}) \qquad (13)$$

$$= 2.63 \times 10^{-4} \text{ in/}^{o}\text{F}$$

13.1.3 Behavior of the Connector When It Is Assembled

The tube diameter of the O-ring is greater than the spacer thickness. The initial bolt load is taken by the O-ring until the O-ring is compressed to the spacer thickness. Ref. 4 gives the seating load for the O-ring used as 1500 lb. per linear inch, or a total bolt load of

$$1500\ (\pi)\ (21.25) = 100{,}000 \text{ lb.}$$

Assume now that this load will be sufficient to make the teflon coating of the O-ring fill up the asperities on the flange surface. Further increase in the bolt load will be taken primarily by the spacer since it is much stiffer than the O-ring. The spacer will be compressed, the bolts stretched and the flanges will roll towards each other. The change in O-ring compression beyond the initial seating compression can be obtained as follows. Assuming that tightening of bolts causes only negligible rolling of the ferrule, then

Decrease in O-ring compression δ_R

$$= (0.2)\ (\text{rotation of integral flange, } \theta) - \text{spacer compression } \delta_s \qquad (14)$$

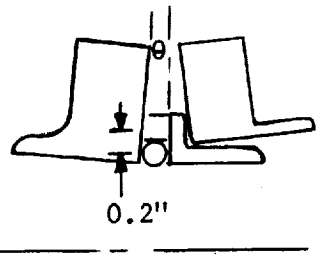

Notice that θ denotes the additional rotation beyond that during initial seating. Eq. (14) can be expressed in terms of the bolt load by using the compliances.

$$\delta_R = 0.2 \left[W - 100{,}000\right] h_G \, q_{FM} - \left[W - 100{,}000\right] q_S$$

$$= \left[W - 100{,}000\right] \left[(0.2)(0.345)(4.81 \times 10^{-7}) - 3.58 \times 10^{-10}\right]$$

$$= \left[W - 100{,}000\right] \left[3.29 \times 10^{-8}\right] \text{in.} \qquad (15)$$

where W = total bolt load and W - 100,000 = spacer load.

It can be seen from this equation that the effect of spacer compression is almost negligible compared with the flange rotation and that tightening the bolts more than is necessary to "seat" the O-ring will always cause a reduction in O-ring compression and the sealing force. To see how much the reduction in sealing force amounts to, we consider that the installation bolt stress is 50,000 psi. For a coarse thread series 7/16 in. nominal diameter bolt, the stress area is 0.106 sq. in. The bolt load per bolt is then

(50,000) (0.106) = 5300 lb.

For 40 bolts the total bolt load is

W = 40 x 5300 = 212,000 lb.

Substituting in Eq. (15) we obtain

$$\delta_R = (212{,}000 - 100{,}000) \quad (3.29 \times 10^{-8}) \qquad (16)$$

$$= 0.00369 \text{ in.}$$

which corresponds to a reduction of sealing force from the initial sealing force of 100,000 lb to

$$100{,}000 - \delta_R \Big/ q_G = 100{,}000 - 0.00369 \Big/ 1.98 \times 10^{-8} \qquad (17)$$

$$< 0$$

This means that separation would occur between the O-ring and the flanges.

13.1.4 Effect of the Load

A. Axial compression of 25,000 lb.

B. Shear of 27,000 lb.

C. Moment of 354,000 lb-in.

The axial compression is transmitted from the ferrule of the steel tube through the spacer to the integral flange. The change in O-ring compression and bolt loads can be found as follows.

The increase in bolt length, $\Delta W q_B$

= The increase in spacer thickness $\Delta H_S \, q_S$

+ The increase in ferrule lip thickness $\Delta H_S \, q_f$

- The decrease in bolt length due to integral flange rotation, $\Delta M \, q_{FM} \, h_G$

- The decrease in bolt length due to loose flange rotation, $\Delta M \, q'_{FM} \, h_G$ (18)

Furthermore, we have the following relation among the load change Δ's.

$$\Delta W + 25{,}000 + \Delta H_s = 0$$
$$\Delta M = \Delta W \, h_G \qquad (19)$$

Using the compliances obtained previously and Eq. (19), Eq. (18) becomes

$$1.92 \times 10^{-8} = - \left(1 + \frac{25{,}000}{\Delta W}\right) (3.58 \times 10^{-10}) \left(\frac{0.145 + 0.312}{0.145}\right) - (0.345)^2 \left[4.81 \times 10^{-7} + 1.82 \times 10^{-6}\right]$$

or $\Delta W = -96.1$ lb.

$\Delta H_s = -24900$ lb. (20)

This shows that the effect of 25,000 lb. is primarily to add to the compression of the spacer. The bolt load, the flange rotation and the gasket sealing force change insignificantly. Next consider the moment of 354,000 lb.-in. The change in the gasket load can be calculated from the method of Section 47. In the present case it assumes the following approximate form.

The max. decrease in gasket load

$$\Delta P_{G\,max} = \frac{M}{\pi \left(\frac{21.25}{2}\right)^2} \cdot \frac{1}{1 + \left(\frac{21.47}{21.25}\right)^2 \left(\frac{q_G}{q_s + q_f}\right) + \left(\frac{22.159}{21.25}\right)^2 \left(\frac{q_G}{q_B}\right)}$$

$$= \frac{354{,}000}{\pi \left(\frac{21.25}{2}\right)^2} \cdot \frac{1}{1 + \left(\frac{21.47}{21.25}\right)^2 \left(\frac{1.98 \times 10^{-8}}{1.13 \times 10^{-9}}\right) + \left(\frac{22.159}{21.25}\right)^2 \left(\frac{1.98 \times 10^{-8}}{1.92 \times 10^{-8}}\right)}$$

= 50.8 lb/in. (21)

which is insignificant in comparison with the initial sealing force of 1500 lb/in.

The corresponding max. decrease in spacer load is

$$\frac{354,000}{\pi\left(\frac{21.47}{2}\right)^2} \quad \frac{1}{1+\left(\frac{21.25}{21.47}\right)^2\left(\frac{1.13 \times 10^{-9}}{1.98 \times 10^{-8}}\right)+\left(\frac{22.159}{21.47}\right)^2\left(\frac{1.98 \times 10^{-8}}{1.92 \times 10^{-8}}\right)}$$

$$= 880 \text{ lb/in.} \qquad (22)$$

which is smaller than the original spacer load. The spacer does not become separated from the flange and the formula we used is valid. We mentioned earlier that tightening the bolts more than is necessary to seat the O-ring is undesirable since it tends to reduce the O-ring compression. But we see now that as far as resisting external moment is concerned, tightening the bolts is desirable, for if the spacer load is negligible, the maximum decrease in gasket load due to the 354,000 lb-in moment would be given by

$$\Delta p_{Gmax} = \frac{354,000}{\pi\left(\frac{21.25}{2}\right)^2} \quad \frac{1}{1+\left(\frac{22.159}{21.25}\right)^2\left(\frac{1.98 \times 10^{-8}}{1.92 \times 10^{-8}}\right)}$$

$$= 463 \text{ lb/in.} \qquad (23)$$

about 9 times the previous value.

The shear of 27,000 lb. does not have much effect on the behavior of the connector because first of all at the point of maximum bending stress, shear vanishes. Furthermore for a spacer load of 112,000 lb. and a coefficient of friction between the steel spacer and the ferrule of 0.4, the maximum friction force to resist the shear is

$$112,000 \times 0.4 = 44800 \text{ lb.}$$

not including the friction between the O-ring and the flanges.

13.1.5 Effect of Internal Pressure of 185 psi

The internal pressure of 185 psi represents an end load of

$$(185)\ (\pi)\left(\frac{20.25}{2}\right)^2 = 65500 \text{ lb.}$$

In addition, it tends to rotate the flanges due to the barreling effect. The change in O-ring compression and bolt loads can be found as follows:

The increase in bolt length, $\Delta W\ q_B$

= the increase in spacer and ferrule lip thickness, $\Delta H_s\ (q_s+q_f)$

- the decrease in bolt length due to integral flange rotation, $\Delta M\ q_{FM}\ h_G$

$$+(185)\ q_{FP}\ h_G$$

- the decrease in bolt length due to loose flange rotation, $\Delta M\ q'_{FM}\ h_G$ (24)

Notice that we have neglected any barreling effect of the loose flange. There exist also the following relations among the load change Δ's.

$$\Delta W - 65{,}500 + \Delta H_s = 0$$
$$\Delta M = \Delta W\ h_G + 65500\ (h_D - h_G) \tag{25}$$

Eq. (24) becomes

$$(1.92 \times 10^{-8}) = \left(\frac{65500}{\Delta W} - 1\right)\ (1.13 \times 10^{-9})$$
$$- (0.345)^2 \left[4.81 \times 10^{-7} + \frac{185}{\Delta W}\ \frac{(3.07 \times 10^{-5})}{0.345} + \frac{(65{,}500)(0.45)(4.81 \times 10^{-7})}{(\Delta W)(0.345)}\right]$$
$$- (0.345)^2 \left[1.82 \times 10^{-6}\right]$$

or

$$\Delta W = -17300 \text{ lb.}$$
$$\Delta H_s = 82{,}800 \text{ lb.} \tag{26}$$

The increase in the integral flange rotation becomes

$$(0.345)(-17300)(4.81 \times 10^{-7}) + (185)(3.07 \times 10^{-5}) + 65500\ (0.45)(4.81 \times 10^{-7})$$
$$= 0.0227 \text{ rad.}$$

The decrease in gasket compression is

$$0.2\ (0.0227) = 0.00454 \text{ in.} \tag{27}$$

due to flange rotation alone. The decrease in gasket compression due to decrease in spacer load of 82,800 lb is

$$(82800)\ q_s = (82800)\ (3.58 \times 10^{-10})$$
$$= 0.00003 \text{ in.} \tag{28}$$

The "would-be" decrease in sealing force is

$$(0.00454 + 0.00002) \Big/ q_G$$

$$= (0.00456) \; / \; (1.98 \times 10^{-8}) \qquad (29)$$

$$= 230{,}000 \text{ lb.}$$

This would have reduced the sealing force to zero and caused separation of the O-ring and flange. Of course the internal pressure has a slight pressure energizing effect. But it can be shown from Section 52 that this effect would increase the O-ring compression of the order of

$$\frac{0.75 \text{ (internal pressure)(tube radius)}^4}{\text{sheet bending rigidity}}$$

$$= \frac{(0.75)(185)\left(\frac{3}{32}\right)^4}{\frac{1}{12\ (1-.3^2)}\ (30 \times 10^6)\ (0.032)^3} \qquad (30)$$

$$= 1.19 \times 10^{-4} \text{ in.}$$

Comparison with Eq. (27) shows that this is far from being sufficient to compensate for the decrease inthe O-ring compression due to flange rotation. This indicates that the connector being considered cannot seal effectively against an internal pressure of 185 psi because of the rotation of the flange, this rotation being mainly due to the barreling effect. At a proof pressure of 1.5 x 185 psi the separation of the O-ring and flange should be even more and there should be even more leakage.

13.1.6 Effect of Low Temperature

In the preceding section we have shown that due to flange rotation leakage is certain to occur at the operating pressure of 185 psi. Account was not taken of the low temperature effect. We shall see whether the low temperature is beneficial or detrimental in this section. Assume that the temperature of the connector drops from a room temperature of 60°F to the cryogenic temperature of -290°F.

The total decrease in flange thickness becomes

$$(60 + 290)\ (K_{Fa} + K'_{F_a}) = (60 + 290)\ (1.05 \times 10^{-5} + 1.05 \times 10^{-5}) \qquad (31)$$

$$= 7.35 \times 10^{-3} \text{ in.}$$

The decrease in bolt length is

$$(60 + 290)\, K_B = (60 + 290)\, (1.32 \times 10^{-5}) = 4.62 \times 10^{-3} \text{ in.} \tag{32}$$

The decrease in spacer and ferrule lip thickness is

$$(60 + 290)\, (1.33 \times 10^{-6})\, \left(1 + \frac{0.312}{0.145} \right) = 1.47 \times 10^{-3} \text{ in.} \tag{33}$$

The change in bolt load and gasket compression due to this differential expansion can be found as follows

The increase in bolt length, $\Delta W\, q_B - 4.62 \times 10^{-3}$

= The increase in spacer and ferrule lip thickness, $\Delta H_s\, (q_s + q_f) - 1.47 \times 10^{-3}$

- The decrease in bolt length due to integral flange rotation, $\Delta M q_{FM}\, h_G$

- The decrease in bolt length due to loose flange rotation, $\Delta M\, q'_{FM}\, h_G$

+ The increase in total flange thickness, -7.35×10^{-3} (34)

Also $\Delta W + \Delta H_s = 0$ (35)

$\Delta M = \Delta W\, H_G$

Therefore, we have

$$\Delta W\, (1.92 \times 10^{-8}) - 4.62 \times 10^{-3} = -\Delta W\, (3.58 \times 10^{-10})(3.15) - 1.47 \times 10^{-3} - \Delta W\, (0.345)^2\, (4.81 \times 10^{-7}) - \Delta W\, (0.345)^2\, (1.82 \times 10^{-6}) - 7.35 \times 10^{-3} \tag{36}$$

or $\Delta W = -14{,}300$ lb.

which is not significant compared with the total bolt load of 212,000 lb. The decrease in the integral flange rotation is

$$(0.345)(-14{,}300)\, (1.99 \times 10^{-7}) = 0.98 \times 10^{-3} \text{ rad.} \tag{37}$$

The corresponding increase in the O-ring compression is

$$(0.2)\ (0.98 \times 10^{-3}) = 0.000196 \text{ in.} \qquad (38)$$

which is not sufficient to compensate for the decrease in the O-ring compression due to the barreling effect given in the preceding section.

13.1.7 Stress Calculations

A. Bolt Stress

The initial bolt stress is 50,000 psi. It has been shown in the preceding sections that the bolt stress changes insignificantly under the loading and temperature environment considered.

B. Flange Stress

(a) Installation Stresses

The maximum stresses in the flanges are given in Ref. 3 as

$$\text{Longitudinal hub stress } S_H = \frac{f M_o}{L g_1^2 B}$$

$$\text{Radial Flange Stress } S_R = \frac{(4/3\ t e + 1) M_o}{L t^2 B}$$

$$\text{Tangential Flange Stress } S_T = \frac{Y M_o}{t^2 B} - Z S_R$$

For the integral flange we can use the method of Ref. 3 to obtain

$f = 1$ $\qquad$ $g_1 = 0.312$

$L = 0.956$ $\qquad$ $e = 0.953$

$Y = 15$ $\qquad$ $Z = 8$

The installation moment is

$$M_o = 100{,}000\ (0.345 + 0.2) + 112{,}000\ (0.345) = 93100 \text{ lb.-in.}$$

Therefore

$$S_H = \frac{93100}{(0.956)(0.312)^2\ (20.25)} = 49400 \text{ psi}$$

$$S_R = \frac{93100\ \left[\frac{4}{3}\ (0.953)(0.875) + 1\right]}{(0.956)(0.875)^2\ (20.25)} = 13300 \text{ psi}$$

$$S_T = \frac{(15)(93100)}{(0.875)^2\ (20.25)} - 8\ (13300) = -16000 \text{ psi}$$

For the loose slip-on flange we have

$f = 1$ $\qquad$ $g_1 = 0.2$

$L = 9.13$ $\qquad$ $e = 1.72$

$Y = 17$ $\qquad$ $Z = 9$

Therefore

$$S_H = \frac{93100}{(9.13)(0.2)^2\ (20.726)} = 12300 \text{ psi}$$

$$S_R = \frac{(93100)\ \left[\left(\frac{4}{3}\right)(0.875)(1.72) + 1\right]}{(9.13)(20.726)(0.875)^2} = 1940 \text{ psi}$$

$$S_T = \frac{(17)\ (93100)}{(0.875)^2\ (20.726)} - 9\ (1940) = 82300 \text{ psi}$$

(b) Stresses under load and low temperature

The maximum stress in the loose flange changes insignificantly under the loading and temperature environment considered. The maximum stress in the integral flange increases due to the barreling effect and decreases slightly due to the low temperature. We have found in Eq. (27) that the increase in flange rotation, due to the 185 psi internal pressure, is 0.0109 rad. The corresponding increase in flange moment is

$$0.0109/q_{FM} = (0.0109)/(1.99 \times 10^{-7})$$

$$= 54800 \text{ lb.-in.}$$

The total maximum stress is

$$49400\left(\frac{93100 + 54800}{93100}\right) = 78{,}500 \text{ psi}$$

which exceeds the yield limit of 6061T6 aluminum alloy at the cryogenic temperature of -290°F. The maximum stress of 82,300 psi in the 7075T6 loose flange is also beyond its yield limit at -290°F.

13.1.8 Conclusion

In the example considered, because the spacer is located inside the bolt circle, rolling of the flanges is of predominating importance. Initial bolt load compresses the O-ring to the spacer thickness and seats the O-ring. Further tightening of the bolts tends to rotate the flange about the spacer and decreases the sealing force. In this respect it is undesirable to tighten the bolts more than necessary. On the other hand, if the bolts are not tightened to the extent that the spacer is heavily loaded, any external moment will have to be taken by the O-ring and the bolts, and there will be large local reduction in sealing force. Because of the smaller rolling rigidity of the flanges, and large rigidity of the spacer, once the connector is tightened any external loads are taken mainly by the spacer; the bolt load remains relatively unaffected. At the operating pressure of 185 psi, the barreling effect will cause the O-ring to separate from the flange. The only possible sealing is now provided by the spacer which is not really intended for this purpose and will not provide a leak-tight joint. Differential thermal contraction at cryogenic temperature reduces the bolt load somewhat and decreases the undesirable rolling of the flange. However, the reduction is insufficient to compensate for the rolling due to internal pressure and cannot make the connector leak tight. The stresses in the flanges are also found to be quite high. It would seem that the use of a spacer inside the bolt circle only is not a desirable design. Alternate designs eliminating the undesirable flange rolling could be achieved by using recessed flanges or a full-depth spacer.

13.1.9 Interpretation of Test Results and Comparison With Theoretical Prediction

After completion of the preceding sections, deformation measurements on the SK20-1286 test fixture were conducted in Huntsville. The general conclusions reached in Section 13.1.8 were fully verified by the test. Some discrepancies exist as to the exact behavior of individual components. In the following we shall make a careful interpretation of the measured data (Ref. 5) and see whether they provide any justification for the many theoretical assumptions.

The first thing that seems to be puzzling about the deformation measurement is that when the bolts are tightened to 285 in-lb the average rolling of the integral flange is (0.0055 + 0.0052 + 0.0065)/3 (5/8) = 0.000917 rad., while the average rolling is still as large as (0.0030 + 0.0021 + 0.0035)/3 (5/8) = 0.000459 rad., when the bolt torque is reduced to 75 in-lb. This indicates

a highly non-linear behavior and there seem to be three possible explanations:

(1) There is already considerable permanent deformation as the bolt torque reaches 285 in-lb.

(2) There is some "backlash" so that the deflection is not measured from true zero.

(3) The behavior is non-linear because at the beginning the bolt load is taken by the incompletely compressed gasket and therefore the moment arm is larger than in the later stages of bolting when the bolt load is carried by the spacer.

Explanation (1) can be ruled out because after retorquing to 285 in-lbs., the rolling of the integral flange is (0.0055 + 0.0062 + 0.0045)/3 (5/8) = 0.000864 rad. which is about the same as that due to initial torque. Most probably it is a combination of (2) and (3) with the effect (3) becoming more important for stiffer gaskets. Based on this understanding we can now calculate the rolling rigidity of the integral flange as

$$\frac{285 - 75}{(0.000917 - 0.000459)} = 4.59 \times 10^5 \text{ in-lb bolt torque/rad.}$$

For the floating flange the average rolling is (0.0100 + 0.0080 + 0.0080)/3(5/8) = 0.00139 rad for the 285 in-lbs. bolt load and (0.0017 + 0.0025 + 0.0025)/3(5/8) = 0.000357 rad. for the 75 in-lbs. bolt load. The bolt load and flange rotation are linearly related, as we should expect. The rolling rigidity is 285/0.00139 = 2.05×10^5 in-lb bolt torque/rad. Therefore the integral flange is 4.59/2.05 = 2.24 times as rigid as the floating flange. This is in contrast to the ratio of 3.71 given in Section 13.1.1. Probable explanations are:

(1) The floating flange does not "float freely" on the steel tube. The steel tube adds to the rigidity of the flange.

(2) Frictional force existing between the flange face and the ferrule lip forms a resisting moment.

The first effect, even if it exists, will be small since the rotation of the floating flange increases insignificantly during pressurization. The second effect of friction, as we shall see, can be quite large. Assuming that the floating flange bears on the tip of the ferrule, the total twisting moment is (total bolt load) x (moment arm = 0.249). If the coefficient of friction between the aluminum flange and the steel ferrule is taken as 0.61, the "maximum" frictional resisting moment that can be developed is
(total bolt load) x (coefficient of friction = 0.61) x (moment arm = 0.875/2) > total twisting moment. Of course, this frictional moment cannot be greater than the active moment, and the actual friction moment can be considerably smaller than the maximum moment. This does show, however, that differential frictional forces at the two flange surfaces can explain the phenomena of the increased "apparent rigidity" of the flanges. For a 3/8 in. nominal diameter fine-thread aluminum bolt, the 285 in-lb bolt torque corresponds roughly to a bolt load of 1000 lb per bolt. Based on this bolt load, the

theoretical rigidity of the integral flange can be calculated as 7.90×10^4 in-lb bolt torque per radian of flange rotation as compared with the apparent rigidity of 4.95×10^5 in-lb bolt torque per radian of flange rotation obtained from the test data. Again the discrepancy is explainable by the frictional interaction with the spacer.

The theoretical result predicts the rotation of the integral flange under 185 psi pressurization to be about three times as large as the flange rotation under 285 in-lb bolt torque. This compares very favorably with the measured value of the ratio of (0.0200 + 0.0.70 + 0.0160)/(0.0055 + 0.0062 + 0.0045 = 3.27 for 200 psi pressurization.

In conclusion it can be said that the test results are in agreement with the general conclusions of our theoretical calculations. Some discrepancies exist as to the exact behavior of the individual components, especially in the increased "apparent rigidity" of the flanges. This can be explained by the existence of frictional force between the flanges and the spacer. It is highly desirable to conduct well designed and controlled tests to investigate further the many assumptions made in the theoretical analysis.

13.2 Flange Joint with Naflex Gasket (by J. Wallach)

13.2.1 Problem

Will the Naflex gasket flanged joint as shown on Ref. 1, and sketched below, leak? If so, what design changes are recommended?

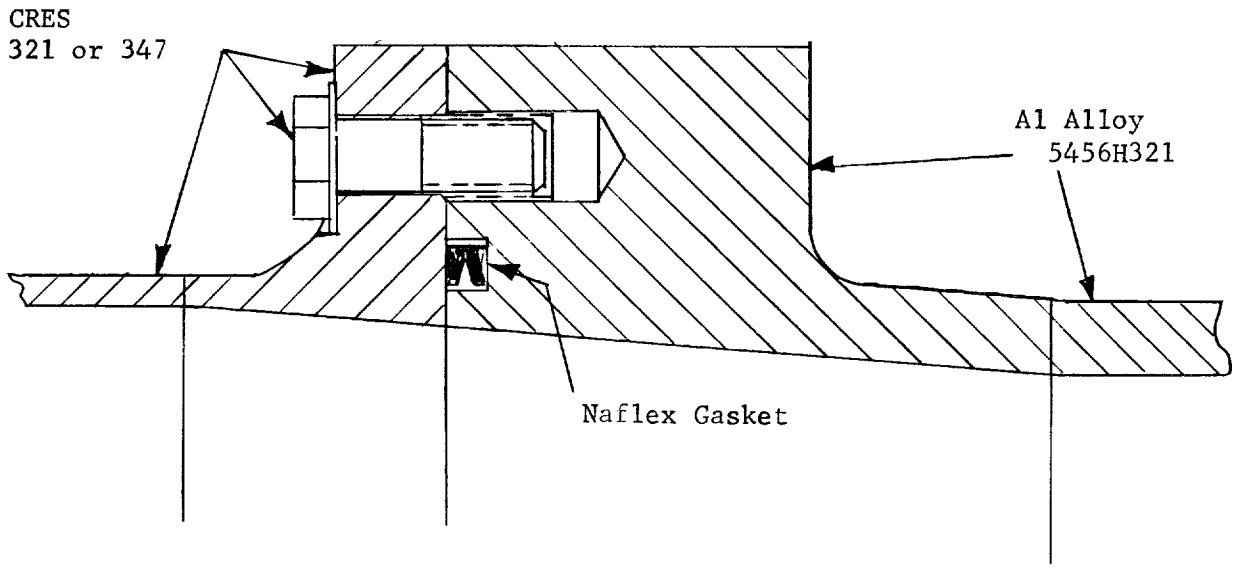

FIGURE 13.2 Flange Joint With Naflex Seal

The determination of whether leakage will occur is to be made for the flanged joint at room temperature and at -290°F, and the same flanged joint at -290°F when both flanges and the bolts are made of aluminum. The operating pressure is 185 psi. The proof pressure is 1.5 times the operating pressure. The maximum axial load on the joint is the proof pressure times the cross-sectional area of the joint, 61,150 lb.

13.2.2 Discussion of Solution

Leakage will occur when the sealing force between the leg of the Naflex seal and flange face is unable to completely force the Teflon coating on the seal into the flange face asperities. This sealing force is developed by the restraint on the seal imposed by the flange faces and the internal pressure. Therefore, the first step in the solution is the determination of the flange separation. Then the seal can be analyzed to determine the seal-to-flange sealing force.

Section 13.2.5.1 of the appendix gives a structural analysis of the flanged joint to determine the angle of flange separation. Based on this analysis, the angle of flange separation was calculated for each case and found to be negligible. The physical dimensions used were those given in Reference 7 and are listed in the appendix, Section 13.2.5.2. The bolt torque is given in Reference 10. The internal pressure is the proof pressure of 278 psi and the axial load is that due to this pressure (61,150 lbs).

As there is no flange separation, the restrained height of the seal is equal to the depth of the recess in the flange. The maximum elastic bending stress calculated in the seal leg due only to this restraint is 254,400 psi (see Section 13.2.5.2 of the appendix). This is well above the yield stress (140,000 to 160,000 psi) for the material. Some yielding can therefore be expected in the seal leg. This will have no subsequent effect on the performance except to improve the initial fit somewhat and broaden the elastic range. A small amount of yielding may be desirable in that a higher sealing force and less critical tolerance requirements will result.

The sealing force between the seal and flange is 81 lb/in. when there is no internal pressure and 98 lb/inch when the pressure is 278 psi. These are the maximum values of sealing force because any manufacturing tolerance on the depth of the flange recess must result in a lower bending stress and therefore lower sealing force after reassembly with different orientations. A tolerance of +.002, -.000 on the recess depth results in a minimum sealing force of 66 lb/in. at zero pressure and 83 lb/in. at 278 psi pressure. Therefore, it is important to maintain small tolerances.

The lip of the seal leg has an 0.006 inch coating of Teflon. The

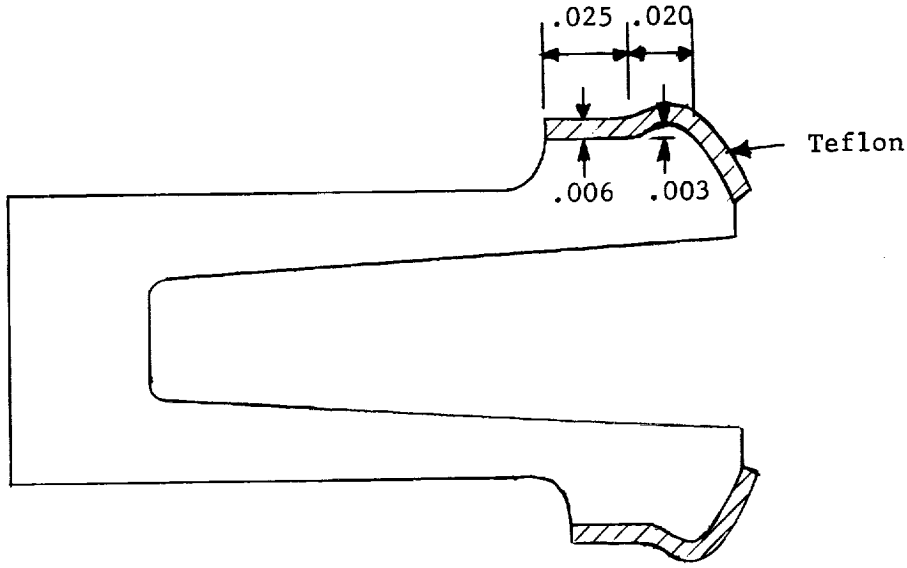

FIGURE 13.3 Cross-section of Naflex Seal Showing Teflon Coating

design of the lip is such that the length of radial contact between the Teflon and flange face increases gradually as the Teflon is plastically deformed. When the radial length of contact reaches .020 inch it has a step increase of .025 inch as the flat part of the lip comes into contact with the flange. If this additional .025-inch length of Teflon were stressed above the yield point, the Teflon would flow plastically away from the seal leg lip. At a sufficiently high load, metal-to-metal contact might occur. To prevent this condition, this additional .025 inch length should not be stressed much above the yield point. Therefore, the length of radial contact for sealing purposes is .020 inch and the stress in the Teflon calculated using the maximum length of radial contact of .045 inch should not be much above the yield stress.

In order to force the Teflon into the asperities on the flange face at room temperature, an initial sealing pressure of about half the 0.2% offset yield stress of the Teflon is required, Section 37.2.4. Once this sealing pressure is attained, the seal will be maintained as long as there is positive contact and no relative motion between the sealing surfaces. Thus, if the .020-inch length is stressed at twice the yield point before the .025-inch length comes into contact, the seal should be maintained at the lower stress level after the .025-inch length comes into contact.

The yield stress of Teflon is about 1000 psi at room temperature and 17,000 psi at -290°F, Ref. 11. At room temperature the sealing force of 66 lb/inch results in a stress of 3300 psi in the .020-inch length and of 1470 psi in the .045-inch length. Also, the sealing force of 98 lb/in. results in a stress of 4900 psi in the .020-inch length and 2180 psi in the .045-inch length. Therefore, an adequate seal is probably effected at the minimum sealing force.

When the seal is installed at room temperature, a seal is effected between the seal and flange face. Once the seal is effected, lowering the temperature can cause relative motion between the seal and flange. At room temperature the differential radial growth is .0056 inch. At -290°F, with the flange and bolt materials as shown on Ref. 7, the differential radial growth is .0193 inch and with both flanges and all bolts of aluminum the differential radial growth is .0230 inch. Therefore, the seal effected at room temperature is always broken when the joint is pressurized. To prevent leakage the Teflon on the seal lip must again be deformed plastically to fill in all the asperities in the flange face after the joint is pressurized. This is possible at room temperature, but not at -290°F. The maximum sealing pressure of 4900 psi is only 29% of the yield stress at this temperature and is not large enough to plastically deform the Teflon. Some leakage is therefore to be expected at -290°F, the amount depending on the initial flatness of the flange surfaces where they come into contact with the Teflon. At room temperature the sealing action should be excellent so long as the seal does not yield enough to give metal-to-metal contact.

13.2.3 Conclusions

The flange joint shown in Figure 13.2 was analyzed to determine whether leakage is likely to occur between the Naflex seal (Fig. 13.3) and flange face. The results of the analysis of the present Naflex seal design are:

1. Leakage is expected at -290°F for each design, the magnitude depending on the flange surface finish.

2. Sealing is excellent at room temperature for each design.

3. Manufacturing tolerances must be kept small because they have a large effect on the ability of the seal to prevent leakage. For example small changes in the depth of the recess in the flange result in large changes in the sealing force between the seal lip and flange face.

4. The sealing force between the seal lip and flange face is large enough to deform plastically the Teflon coating on the seal lip at room temperature, but not at -290°F.

5. There is relative motion between the seal lip and flange face when the joint is pressurized and chilled.

6. The two-part seal-lip design of Fig.13.3 is a desirable feature. One part protrudes above the other and it is this part of the Teflon coating that is deformed plastically by the flange face to fill the asperities in the flange face and prevent leakage. The second part comes in contact with the flange face after the first part is plastically deformed and by increasing the area decreases the rate of further increase of contact stress of the Teflon at the sealing point. In this way metal-to-metal contact between the seal leg and flange face is largely prevented.

13.2.4 Nomenclature

		Units
a	Thermal strain	inch/inch
A_3	Cross-sectional area of bolt	$inch^2$
b	Length, radial	inch
D	Flexural rigidity	inch lb
E	Modulus of elasticity	psi
f	Force	lb
F	Force per inch of circumference	lb/in
g	Coefficient of friction	
h	Length, axial	inch
m	Moment	inch lb
M	Moment per inch of circumference	inch lb/inch
n	Number of threads per inch	threads/in
N	Axial force per inch of circumference	lb/inch
p	Pressure	psi
Q	Shear	lb/inch
r	Radius	inch

Nomenclature (continued)

		Units
R_s	Sealing force between seal and flange	lb/inch
S_y	Yield stress	psi
t	Thickness	inch
T	Torque	inch lb
w	Deflection	inch
y_o	Deflection of sealing end of seal leg	inch
β	Angle between a line normal to the thread surface at the pitch radius and a line parallel to the thread axis.	radian
θ	Angle	radians
ν	Poisson's ratio	
σ_h	Hoop stress in seal web	psi
σ_m	Maximum bending stress in seal leg	psi
ϕ	One-half of included angle of thread, measured in a plane which includes the thread axis	radian

13.2.5 Appendix

13.2.5.1 Flanged Joint Analysis

The flanged joint analysis is directed toward the determination of the flange face separation at the Naflex gasket. The flange separation is then used to determine the sealing force between the Naflex gasket leg and the flange face. A consideration of the material coating on the seal leg and the sealing force will determine whether leakage will occur. Another factor is the maximum stress in the seal leg. This is also a function of the flange face separation and the internal pressure.

The flanged joint is detailed on the "Naflex Gasket Test Fixture" drawing, Ref. 7. The analysis is reduced to a consideration of the two flanges, two adjoining pipes and the bolts. The test fixture flanged joints are at a sufficient distance from the test joint so as not to affect appreciably the structural response of the test joint. The external loads on the test joint are the internal pressure, axial force, transverse bending moment, and transverse shear. The test joint will be loaded at room temperature and -290°F.

The external loading may be reduced to an internal pressure and axial force. The transverse bending moment on the pipe may be represented by an axial force varying sinusoidally along the circumference of the pipe.

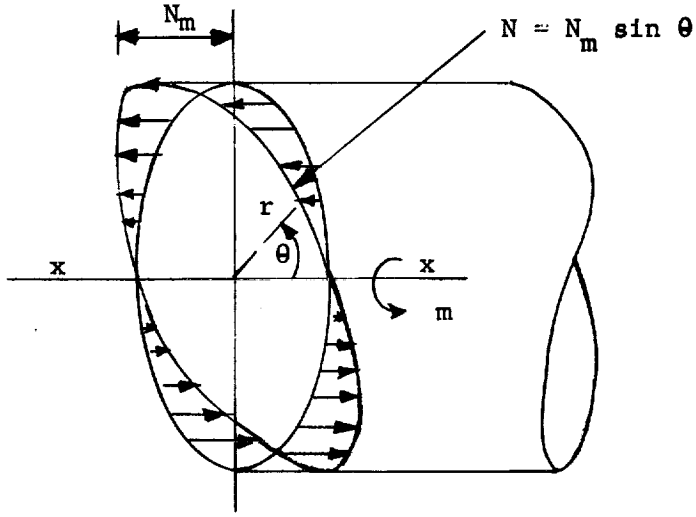

FIGURE 13.4 Transverse Bending Moment on Pipe

The moment about the x-x axis, m, is equal to the integral of the axial force N times its distance from the x-x axis.

$$m = \int_0^{2\pi} (N_m \sin \theta)(r \sin \theta) r d\theta$$

The maximum axial force, N_m, is found from the above equation.

$$N_m = m/\pi r^2 \qquad (1)$$

The point of maximum flange separation is the point where leakage is most likely to occur. From a consideration of the forces, this is the point where the axial force is a maximum in tension. Therefore, the net axial force and the maximum axial force, N_m, due to the transverse moment may be combined (see Section 47). This total axial force is then considered to be acting along the whole pipe circumference. The transverse shear is distributed over the pipe cross-section in a manner that will not appreciably affect the flange separation and therefore is neglected.

The total axial force, f_A, is related to the force per inch of circumference of each cylinder. This relation is used

$$f_A = 2\pi r_1 F_1 = 2\pi r_5 F_5 \qquad (2)$$

in the equations to substitute f_A for F_1 and F_2.

Deflection and rotation equations are written for each cylinder and flange, and an equation is written for the bolt elongation. The radial deflections of the cylinders and flanges are the same. The rotation of cylinder (1) and flange (2) are the same. The rotation of cylinder (5) and flange (4) are the same. The difference between the rotation of flange (4) and flange (2) is the angle of flange separation, θ_3. The bolt elongation is related to the flange separation. The forces and moments on each side of a juncture of a cylinder to a flange are equal and opposite. The forces on opposite

flanges and on adjoining surfaces of the bolt and flange are equal and opposite. Note the subscripts on Figure 13.5 indicate the equivalence of deflections, rotations, forces and moments.

A set of ten linear equations are written which can be solved simultaneously for w_1, θ_1, θ_3, M_1, M_5, Q_1, Q_5, F_2, F_3 and F_6. The equations for the deflection and rotation of cylinder (1) due to an edge shear and moment are given by equations (279) and (280) of Ref. 8. Additional terms are added to the deflection equation to account for the deflection due to internal pressure and thermal expansion.

$$w_1 = \left(\beta_1 M_1 + Q_1\right)/2\beta_1^3 D_1 + r_1\left(pr_1 - \nu_1 f_A/2\pi r_1\right)/t_1 E_1 + a_1 r_1 \tag{3}$$

$$\theta_1 = \left(2\beta_1 M_1 + Q_1\right)/2\beta_1^2 D_1 \tag{4}$$

where

$$D_1 = E_1 t_1^3/12\left(1 - \nu_1^2\right) \tag{5}$$

$$\beta_1^4 = 3\left(1 - \nu_1^2\right)/r_1^2 t_1^2 \tag{6}$$

The radial deflection of flange (2) is also w_1 and is due to the internal pressure, radial shear forces and thermal expansion.

$$w_1 = \left(r_1/t_2 E_2\right)\left[pr_1 - Q_1 r_1/h_2 + F_6\left(r_1 + b_2 + b_3\right)/h_2 + \nu_2 F_3\left(r_1 + b_1 + b_2 + b_3\right)/\left(r_1 + b_3\right)\right] + r_1 a_2 \tag{7}$$

The sum of the forces acting on the flange (2) in the axial direction must be zero.

$$F_1 r_1 - F_2\left(r_1 + b_2 + b_3\right) + F_3\left(r_1 + b_1 + b_2 + b_3\right) = 0 \tag{8}$$

The rotation of the flange (2) is not coupled with the radial deflection. It is further assumed that the flange acts like a ring. That is, there is no distortion of the cross-section. To verify this, a calculation of the bending of the flange (2) was made using the formulas of Section 43.3, for a flat flange. Considering only the reactive force between the flange faces, F_3, the bolt load, F_2, and the axial load, F_1, an angular rotation of the innermost part of the flange with respect to the outer part of the flange of 5×10^{-4} radians was calculated. This is quite small and is neglected in this analysis. The rotation of the ring cross-section is given by equation (126) of Ref. 9.

$$\left[t_2 h_2^3 E_2/12\left(r_1 + b_3\right)^2\right]\theta_1 = -M_1 + h_2 Q_1/2 - b_2 F_2 + \left(b_1 + b_2\right)F_3 + h_2 F_6/2 - b_3 f_A/2\pi r_1 \tag{9}$$

The difference between the rotation of flange (2) and flange (4) is the angle of flange separation, θ_3. The outside radii of the flanges is the same and their radial deflections are the same. The flanges separate by rotating about a point close to their outside radii. There is a small area of contact in which it is assumed the stresses are in the plastic region. F_3 acts

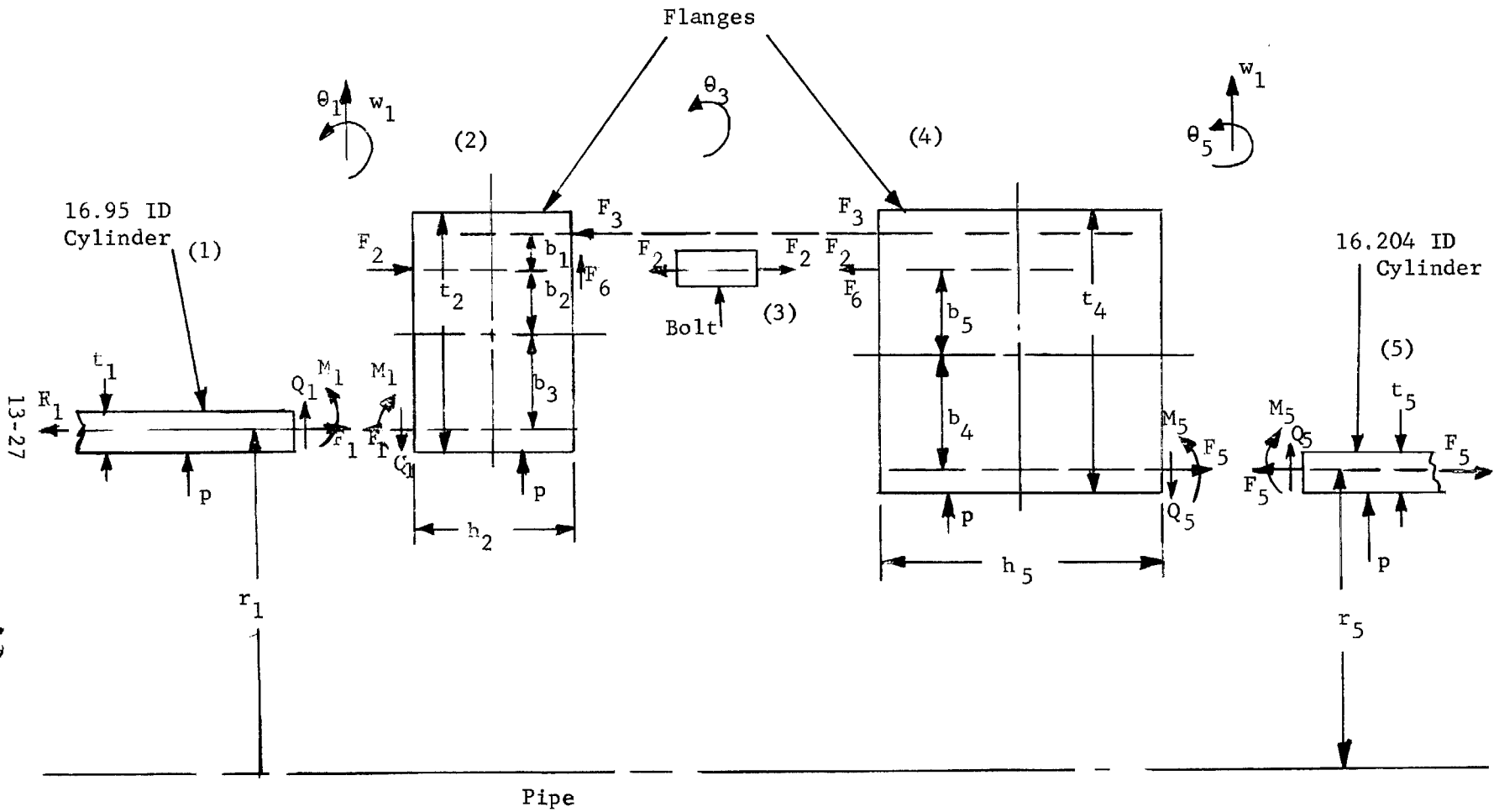

FIGURE 13.5 Flanged Joint Separated into Elements

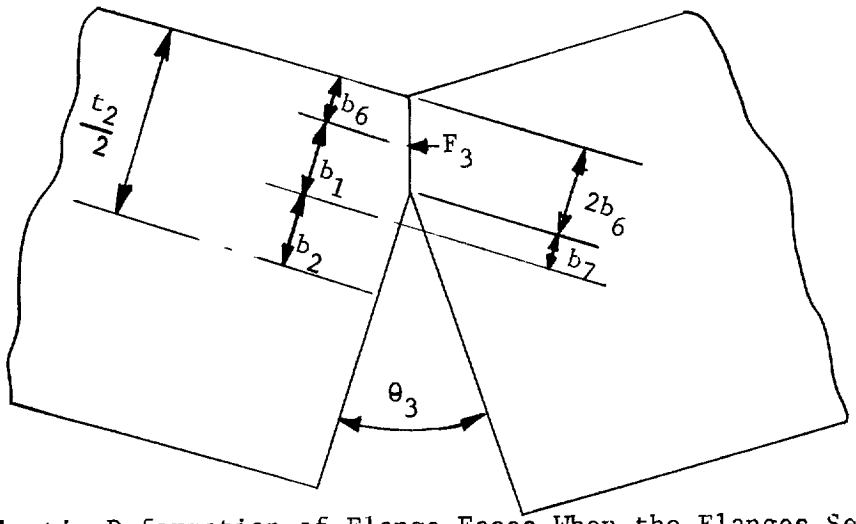

FIG. 13.6 Plastic Deformation of Flange Faces When the Flanges Separate

in the center of the region. θ_3 is small and cos θ_3 is approximately one.

$$S_y = F_3/2b_6 \tag{10}$$

$$b_6 + b_1 + b_2 = t_2/2 \tag{11}$$

Solving for b_1:

$$b_1 = t_2/2 - b_2 - F_3/2Sy \tag{12}$$

Equation (12) may be used to calculate the value of b_1 to be used in the calculations.

$$2b_6 + b_7 + b_2 = t_2/2 \tag{13}$$

From equations (11)and (13):

$$b_7 = 2b_1 + b_2 - t_2/2 \tag{14}$$

b_7 is the distance of the bolt from the center of rotation of flange separation.

The angle of flange separation is equal to the bolt elongation divided by the distance of the bolt from the point of rotation. The bolt elongation depends on the total bolt force per inch of circumference, F_2, the initial bolt force per bolt, f_B, and the thermal elongation of the bolt.

$$\theta_3 = \left(h_3/A_3E_3\right)\left[2\pi F_2\left(r_1 + b_2 + b_3\right)/36 - f_B\right]/\left(2b_1 + b_2 - t_2/2\right) + h_2\left(a_3 - a_2\right)/\left(2b_1 + b_2 - t_2/2\right) \tag{15}$$

The rotation of flange (4) is equal to the rotation of flange (2) plus the flange separation. Flange (4) is considered

$$\theta_5 = \theta_1 + \theta_3$$

a ring and the rotation of the cross-section is given by equation (126) of Ref. 9.

$$\left[t_4 h_4^3 E_4/12\left(r_5 + b_4\right)^2\right]\left(\theta_1 + \theta_3\right) = M_5 - h_4 Q_5/2 + b_2 F_2 - \left(b_1 + b_5\right)F_3 + h_4 F_6/2 + b_4 f_A/2\pi r_5 \qquad (16)$$

The radial deflection of flange (4) is equal to that of flange (2). It is due to the internal pressure, radial shear forces and thermal expansion.

$$w_1 = \left(r_5/t_4 E_4\right)\left[pr_5 - Q_5 r_5/h_4 - F_6\left(r_5 + b_4 + b_5\right)/h_4 - \nu_4 r_5 F_5/\left(r_5 + b_4\right)\right] + r_5 a_4 \qquad (17)$$

The radial deflection of the edge of cylinder (5) is also equal to w_1 and due to the internal pressure, edge shear and thermal expansion.

$$w_1 = \left(\beta_5 M_5 + Q_5\right)/\left(2\beta_5^3 D_5\right) + \frac{r_5}{t_5 E_5}\left(pr_5 - \nu_5 F_5\right) + a_5 r_5 \qquad (18)$$

The rotation of the edge of cylinder (5) is the same as that of flange (4).

$$\theta_1 + \theta_3 = -\left(2\beta_5 M_5 + Q_5\right)/\left(2\beta_5^2 D_5\right) \qquad (19)$$

where

$$D_5 = E_5 t_5^3/12\left(1 - \nu_5^2\right) \qquad (20)$$

$$\beta_5^4 = 3\left(1 - \nu_5^2\right)/r_5^2 t_5^2 \qquad (21)$$

The simultaneous solution of equations (3), (4), (7), (8), (9), (15), (16), (17), (18) and (19) will give the flange separation θ_3, as shown in the next section.

13.2.5.2 Naflex Gasket Test Fixture Calculations

In order to determine whether the flange will leak it is necessary to determine if a tight seal is made, and maintained, between the Naflex gasket and flange face. An important parameter in this determination is the sealing force between the Naflex gasket and flange face. This sealing force is a function of the internal pressure and restrained axial height of the gasket. The initial restrained height of the gasket is determined by the depth of the recess in the flange face as given on Ref. 7. The increase in the gasket height when the flanged joint is loaded depends upon the amount of flange separation. This can be calculated using the equations derived in part 1 of this appendix.

Before calculating the angle of flange separation, θ_3, the axial force, f_A, and bolt load, f_B, must be calculated. The dimensions for the flanged joint are given on Ref. 7.

A_3 = .1486 inch^2
b_2 = .172 inch
b_3 = .528 "
b_4 = .638 "
b_5 = .213 "
g = .12
h_2 = .625 inch
h_3 = .8 "
h_4 = 1.87 "
n = 20
p = 278 psi (1.5 times operating pressure of 185 psi for proof test)
r_1 = 8.55 inch
r_5 = 8.399 "
t_1 = .1495 inch
t_2 = 1.405 "
t_4 = 1.487 "
t_5 = .375 "
T = 475 inch-lb (Steel bolt, Ref. 10)
= 285 " (Aluminum bolt, Ref.10)
ϕ = 30 degrees

The material properties are given in Ref. 11. These are not the exact properties of the materials used, as the materials used and the materials for which properties are available are not specified precisely. However, the properties are sufficiently accurate for the calculations.

Material	Temperature	E	ν	a	Sy
Steel -347	68°F	29 x 10^6 psi	.284	0	62,000 psi
	- 290°F	29 x 10^6	.28	.0027	65,000
Aluminum 5456	68°F	10 x 10^6	.343	0	39,000
	- 290°F	11 x 10^6	.33	.0037	45,000

The axial force acting on the test flange is equal to the proof pressure times the area. This force is 61,150 lb. In service the joint is subjected to a transverse bending moment of 350,000 inch-lb and a compressive axial load of 25,000 lb. At the point of maximum axial tensile force due to the bending moment alone, the equivalent axial force is $2\pi r N_m$ where N_m is given by equation (1). The equivalent axial force of 83,580 lbs. minus the compressive load of 25,000 lb gives a maximum of 58,580 lb. As the proof test load is larger, it is used in the calculations (f_A = 61,150 lb.).

The length b_1 is estimated here although a direct calculation might be made as shown in Section 41.3. Consider flange (2) loaded only by F_1 and F_3. Then the sum of the moments about the point of application of F_2 gives:

$$b_1 F_3 - (b_2 + b_3) F_1 = 0 \qquad (22)$$

Substituting for F_1 from equation (2), for F_3 from equation (12) and solving for b_1 gives:

$$b_1 = .25\left|t_2 - 2b_2\right| + .5\sqrt{.25(t_2 - 2b_2)^2 - f_A(b_2 + b_3)/(r_1\pi S_y)} \qquad (23)$$

In calculating b_1 the yield stress of the softer material is used.

S_y, psi	b_1, inch
39,000	.5100
45,000	.5127

The initial bolt load, f_B, is calculated using the formulas for "The total tension in a bolt" on page 239 of Ref. 13.

f_B = 6790 lb for steel bolts

f_B = 4080 lb for aluminum bolts

The flange separation, θ_3, is calculated for three cases.

Case	
1	Flange materials as shown on Ref.7 at room temperature.
2	" " " " " " " " -290°F
3	Flange materials both aluminum at -290°F

Equations (3), (4), (7), (8), (9), (15), (16), (17), (18) and (19) are solved simultaneously for the flange separation.

Case	θ_3, Radians	w_1, Inches
1	-.00196	.0011
2	-.00163	-.0263
3	-.00280	-.0300

The results show that there is no flange separation in any case. A negative angle shows that the equations have been applied beyond their range of validity and thus merely indicates the flange faces are in full contact.

The Naflex gasket used in the test flange has a dash number of -367. The material is 4340 steel and the major dimensions are given in the diagram below. These are nominal dimensions taken from the Naflex Drawing. Some of the dimensioning has been changed to make it consistent with the nomenclature used in the analysis.

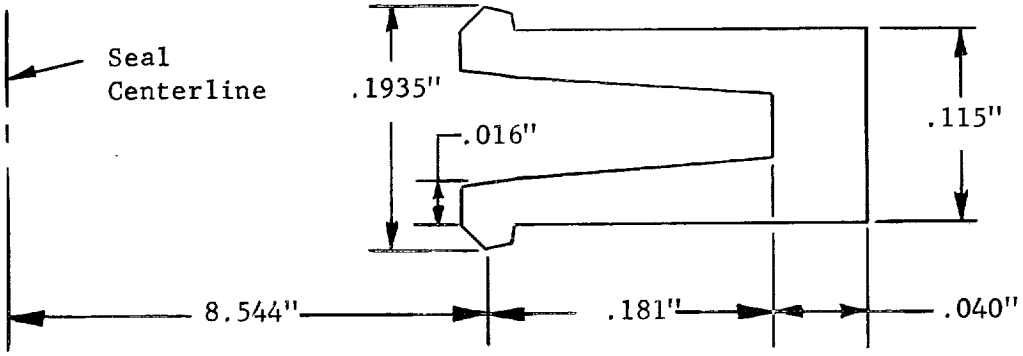

FIG. 13.7 Nominal Dimensions of Seal Cross-section

The restrained height of the seal is given in Ref. 7 as .174". As there is no flange face separation, this height remains constant when pressure is applied. Substituting the geometric parameters in equations (15), (18) and (20) of Section 51.5.2 the following equations for the sealing force R_s and maximum stress, σ_m, are obtained.

$$R_s = -15{,}070\ y_o + .06317\ p \tag{24}$$

$$\sigma_m = 2.609 \times 10^7\ y_o + 47.3\ p \tag{25}$$

y_o is the deflection of the seal leg due to the restraint of the flange faces. This is -.00975" for the design shown on Ref. 7.

The maximum stress for y_o = -.00975 in. and p = 0 is -254,400 psi which is well above the yield point of the seal material. The yield stress of 4340 steel is 140,000 to 160,000 psi, Ref. 6. Based on the yield stress of 140,000 psi and with zero pressure the sealing force calculated using equations (24) and (25) is 81 lb/in. The internal pressure of 278 psi raises this force to 98 lb/in. A change in the recess depth of .002" results in a change in y_o of .001" and a change in the sealing force of 15 lb/in.

The radial deflection of the seal leg due to the internal pressure of 278 psi is calculated using equation (55) of Section 51.5.5 to be .0067 inch. The hoop stress in the seal web is calculated as described in Section 51.5.4.

$$\sigma_h = pr/t = 60{,}780 \text{ psi} \tag{26}$$

The radial contraction of the seal due to the drop in temperature to -290°F is calculated using the coefficient of thermal expansion from Ref. 11. The radial contraction is -.0137 inches. Therefore, the relative radial motion of the seal to the flange is:

Case	Relative Radial Motion, inches
1	.0056
2	.0193
3	.0230

The effect of frictional forces between the seal lip and flange face is small. The coefficient of friction for Teflon to steel is approximately .05, Ref. 14. Using the maximum sealing force of 98 lb/inch, for the modified seal recess, a radial frictional force of 9.8 lb/inch acts at the circumference of the gasket. An equivalent pressure acting over the .1935 inch axial length of the seal would be equal to 51 psi. The radial deflection due to this pressure is approximately .0012 inch as calculated using equation (55) of Section 51.5.5. This maximum value of radial deflection is small by comparison to the values in the above table. Therefore, the decrease in the relative radial deflection of the seal with respect to the flange faces due to the frictional force between the seal and flange may be neglected.

13.3 Flange Test Model, MC Fitting (by C.H. Gay)

13.3.1 Introduction

The modified MC type flanged connector described in NASA-Huntsville drawing SK20-1501 has been analyzed for leakage characteristics. It was found that for the prescribed loading conditions large-scale leakage would be present using aluminum bolts. Using steel bolts a maximum leakage in the order of 0.02 lb of helium per hour is obtained.

The test model configuration, shown schematically in Fig. 13.8 was analyzed for the specific cases of:

(1) elememts "a" and "b" composed of 347 stainless steel; elements "c", "d" and "e" composed of Al 2219-T6, and

(2) the coupling bolts composed of either material.

The operating conditions of interest were:

(1) enclosed helium at 1500 psi and 125°F

(2) in addition, external liquid oxygen at 60 psi and -293°F and

(3) after condition 2 is stabilized, increase helium pressure to 3200 psi.

The analysis will be directed toward determination of the normal sealing force from which the leakage rate is estimated.

13.3.2 Assumptions

The actual connector assembly was reduced to the model shown in Fig. 13.8 and then separated into sections "a" through "e," Fig. 13.9, for analysis of forces.

Detailed analysis of leakage required that several simplifying assumptions be made:

(1) Elements a and d of the connector itself are treated as long cylinders.

(2) Rings b, c and e are sufficiently large that they rotate without cross-sectional distortion.

(3) The connector loadings have no significant effect on the sealing point location.

(4) All materials are homogeneous and isotropic. Stresses (except those at the sealing point) are below the proportional limit.

(5) Bolt loads can be treated as a uniform line load acting at the bolt circle. Bolt holes are neglected in centroid calculations.

(6) Strain hardening effects are considered negligible.

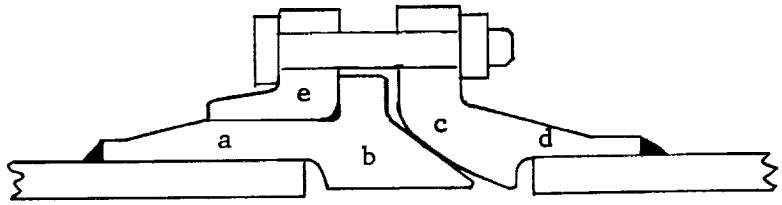

FIGURE 13.8
Connector Assembly

47

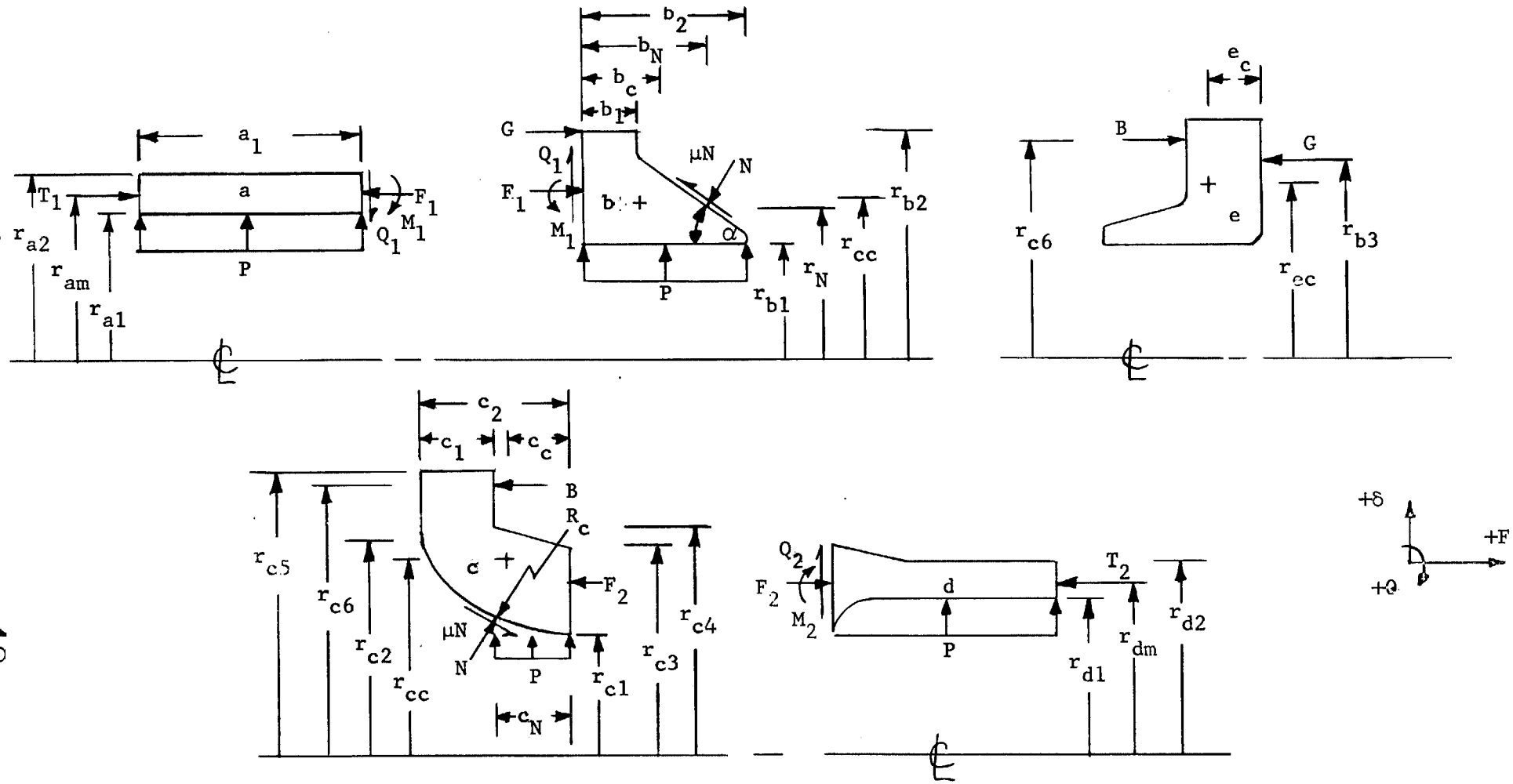

Dimensions:

r_{a1}	= 2.010	r_{c1}	= 1.68	r_{ec}	= 2.912	a_1	= 2.450	c_1	= .700
r_{a2}	= 2.460	r_{c2}	= 2.509	α	= 37°	b_1	= .590	c_2	= 1.25
r_{am}	= 2.235	r_{c3}	= 2.495			b_2	= 1.550	c_N	= .80
r_{b1}	= 1.650	r_{c4}	= 2.642			b_c	= .571	c_c	= .679
r_{b3}	= 2.885	r_{c5}	= 3.512			b_N	= .757	R_c	= 1.83
r_N	= 2.02	r_{c6}	= 3.106					d_1	= 1.25
r_{bc}	= 2.134	r_{cc}	= 2.619					e_c	= .516
		r_{d1}	= 2.01						
		r_{d2}	= 2.31						
		r_{dm}	= 2.16						

FIGURE 13.9 Connector Details

13.3.3 Nomenclature

a,b,c,d,e	=	connector elements	
B	=	effective bolt load	lb/in.
G	=	bolt load reaction on ring 'b'	lb/in.
F_i, T_i	=	axial loads	lb/in.
N	=	normal sealing force	lb/in.
Q_i	=	shear force	lb/in.
M_i	=	bending moments	in. lb/in.
P	=	internal pressure	$lb/in.^2$
θ	=	angular rotation	radians
δ	=	radial displacement	inches
Δ	=	axial displacement	inches
$\Delta\Delta$	=	change in axial displacement	inches
r	=	radius of a connector element	inches
R_c	=	radius of curvature of ring 'c' sealing contour	inches
k	=	$(1 - \nu^2)/\pi E$ = elastic property of sealing surface	in^2/lb
$w_{elas.}$	=	axial width of seal area of unit circumferential length	in^2/lb
$\sigma_{elas.}$	=	maximum contact stress	lb/in^2
$\sigma_{eff.}$	=	uniform contact stress	lb/in^2
$w_{eff.}$	=	axial width acted on by uniform stress	in^2/in
h_r	=	effective individual surface roughness in direction of flow	10^{-6} in.
h_e	=	effective leakage flow path height	10^{-6} in.
Q_u	=	uncorrected flow rate	lb/hr
Q	=	corrected flow rate	lb/hr
T	=	actual gas temperature	^oF
ν_i	=	Poisson's ratio	
E_i	=	modulus of elasticity	lb/in^2
α_i	=	coefficient of thermal expansion	$1/^oF$
μ_i	=	" " static friction	
A	=	cross-section, area	in^2
I	=	moment of inertia about radial axis	in^4

13.3.4 Determination of Sealing Force

From Fig. 13.9, equilibrium conditions on ring 'e' require:

$$\Sigma F_x = 0 = 2\pi\, r_{c6}\, B - 2\pi\, r_{b3}\, G$$

$$G = B\, \frac{r_{c6}}{r_{b3}} \qquad (1)$$

Also for ring "b"

$$\Sigma F_x = 0 = 2\pi\, r_{b3}\, G + 2\pi\, r_{am}\, F_1$$

$$- 2\pi\, r_N\, N \sin\theta - 2\pi\, r_n\, \mu\, N \cos\theta \qquad (2)$$

Substitution of Eq. (1) in (2) yields

$$r_{c6}\, B + r_{am}\, F_1 - r_N\, N\, (\sin\theta + \mu_N \cos\theta) = 0$$

Substituting radius and θ values and solving for N

$$N = \frac{1.54B + 1.11\, F_1}{.601 + .798\, \mu_N} \qquad (3)$$

If the bolt load B were not affected by the motion of the connector sections, sealing load could be determined directly from Eq. (3). However, load effects on B must be considered.

13.3.5 Rotation and Deflection Equations

13.3.5.1 Cylinder 'a', Fig. 13.9

We consider positive radial displacement outward and positive angular rotation clockwise. We denote deflection by δ with suitable subscript and rotation by θ with suitable subscript. Then the deflection and rotation of cylinder 'a' at its junction with ring 'b' is given by (see Section 42, Eqs. 18 and 19)

$$\delta_a = -\left[2\, r_{am}^2\, \beta_a^2 / E_s \left(r_{a2} - r_{a1}\right)\right] M_1$$

$$-\sqrt{1 + 0.59\, \left(r_{a2} - r_{a1}\right)/r_{am}}\left[2 r_{am}^2\, \beta_a / E_s \left(r_{a2} - r_{a1}\right)\right] Q_1$$

$$+ \left[r_{am}/E_s\, \left(r_{a2} - r_{a1}\right)\right]\left[P r_{a1} + \nu F_1\right] \qquad (4)$$

$$\theta_a = \sqrt{1 + 0.59\left(r_{a2} - r_{a1}\right)/r_{am}}\left[4r_{am}^2\beta_a^3/E_s\left(r_{a2} - r_{a1}\right)\right] M_1$$

$$+ \left[2r_{am}^2\beta_a^2/E_s\left(r_{a2} - r_{a1}\right)\right] Q_1 \qquad (5)$$

where

$$\beta_a = \frac{\sqrt[4]{3(1 - \nu^2)}}{\sqrt{r_{am}\left(r_{a2} - r_{a1}\right)}} = 1.282 \text{ in}^{-1}$$

since

$r_{a2} = 2.46$ in.
$r_{a1} = 2.01$ in.
$r_{am} = 2.23$ in.
$\nu = 0.3$ (assumed value)

with $E_s = 28,200,000$ lb/in^2 Eqs. (4) and (5) becomes

$$10^6\delta_a = - 1.289 M_1 - 1.061 Q_1 + 0.353 P + 0.0527 F_1 \qquad (6)$$

$$10^6\theta_a = 3.49 M_1 + 1.289 Q_1 \qquad (7)$$

13.3.5.2 Cylinder 'd', Figure 13.9

For this cylinder we ignore the taper at the junction with ring 'c' and use $\nu = 0.3$ again

$r_{dm} = 2.16$
$r_{d2} = 2.31$ in.
$r_{d1} = 2.01$ in.
$\beta_d = 1.598$ in^{-1}

With a modulus of 10,600,000 psi for the aluminum we get, comparable to Eqs. (6) and (7)

$$10^6\delta_d = 7.50 M_2 + 4.88Q_2 + 1.365P + .204F_2 \qquad (8)$$

$$10^6\theta_d = 24.95M_2 + 7.50Q_2 \qquad (9)$$

13.3.5.3 Ring 'b', Figure 13.9

The moment of inertia I_b of the ring cross-section about a vertical axis through the centroid is 0.1937 in^4. The moment M_T (Eq. (1) of Section 42) is obtained in terms of the loads G, F_1, N, μN, M_1, Q_1 and P by use of the free body diagram of the half ring (upper figure of Fig. 42.1) as

$$M_{Tb} = r_{b3}^2 G + r_{am}^2 F_1 - r_N^2 N\left(\sin\alpha + \mu\cos\alpha\right) - r_{b1} b_N P\left(b_N/2 - b_c\right) + r_{am} b_c Q_1$$

$$+ r_N\left(b_N - b_c\right) N\left(\cos\alpha - \mu\sin\alpha\right) - r_{am} M_1 \qquad (10)$$

with $r_{b3} = 2.885$ in.

$r_{am} = 2.235$ in.

$r_N = 2.02$ in.

$\alpha = 37^o$

$\mu = \pm 0.6$ (estimated for steel on aluminum from Ref. 13. Sign depends on relative motion and for no motion the effective μ can be anywhere between +0.6 and -0.6)

$r_{b1} = 1.650$ in.

$b_N = .757$ in.

$b_c = .571$ in.

In deriving Eq. (10) we have taken the friction force that accompanies G to be negligible due to lubrication.

Substituting values in Eq.(10) gives ($\mu = +0.6$)

$$M_{Tb} = 8.33G + 5.00F_1 - 4.25N + .240P + 1.277Q_1 - 2.235M_1 \qquad (11a)$$

The twist of ring 'b' is given by Eq. (6) of Section 42 as

$$\theta_b = M_{Tb} r_{bc} / E_s I_b \qquad (12)$$

with $r_{bc} = 2.134$ in.

$E_s = 28,200,000$ lb/in^2

$I_b = 0.1937$ in.

$$10^6 \theta_b = 0.390 M_{Tb} \qquad (13)$$

With Eq. (11) we have

$$10^6 \theta_b = 3.25G + 1.95F_1 - 1.66N + .0937P + .498Q_1 - .873M_1 \qquad (14a)$$

The radial deflection of ring 'b' at its centroid is given in Eq. (14) of Section 42 as

$$\delta_b = r_{bc} r_{b1} P b_n / E_s A_b + r_{bc} r_{am} Q_1 / E_s A_b - r_{bc} r_N N(\cos \alpha - \mu \sin \alpha)/E_s A_b \qquad (15)$$

where $A_b = 1.227$ in^2 (cross-sectional area of ring 'b'). Substituting values into Eq. (15)

$$10^6 \delta_b = .0771P + .1380Q_1 - .0545N \qquad (16a)$$

Repeating Eqs. (11), (14) and (16) for $\mu = -0.6$ gives

$$M_{Tb} = 8.33G + 5.00F_1 - .06N + .240P + 1.277Q_1 - 2.235M_1 \qquad (11b)$$

$$10^6\theta_b = 3.25G + 1.95F_1 - .018N + .0937P + .498Q_1 - .873M_1 \quad (14b)$$

$$10^6\delta_b = .0771P + .1380Q_1 - .1443N \quad (16b)$$

13.3.5.4 Ring 'e', Fig. 13.9

For this ring the equations similar to (11) through (16) are obtained. First

$$M_{Te} = - r_{b3}^2 G + r_{c6}^2 B \quad (17)$$

where

r_{b3} = 2.885 in.

r_{c6} = 3.106 in.

Substituting values into Eq. (17)

$$M_{Te} = - 8.33G + 9.65B \quad (18)$$

The twist is given by

$$\theta_e = M_{Te} r_{ec}/E_A I_e \quad (19)$$

where r_{ec} = 2.912 in.

I_e = 0.132 in^4

E_A = 10,600,000 lb/in^2

Substituting values in Eq. (19) gives

$$10^6\theta_e = 2.080\ M_{Te} \quad (20)$$

with Eq. (18) we have

$$10^6\theta_e = - 17.30G + 20.05B \quad (21)$$

There are no radial forces on ring 'e' so its radial growth is zero at its centroid.

$$10^6\delta_e = 0 \quad (22)$$

13.3.5.5 Ring 'c', Fig. 13.9

For this ring the equations similar to (11) through (16) are obtained, First

$$M_{Tc} = - r_{c6}^2 B - r_{dm}^2 F_2 + r_N^2 N\ (\sin\alpha + \mu\cos\alpha) - r_{dm} M_2 + r_{c1} c_N P(C_N/2 - C_c)$$

$$+ r_{dm} C_c Q_2 + r_N (C_N - C_c) N(\cos\alpha - \mu\sin\alpha) \quad (23)$$

with $r_{c6} = 3.106$ in.
$r_{dm} = 2.16$ in.
$r_N = 2.02$ in.
$\alpha = 37^o$
$r_{c1} = 1.68$ in.
$C_N = 0.800$
$C_c = 0.679$

we get for $\mu = 0.6$

$$M_{TC} = - 9.65B - 4.66F_2 + 4.52N - 2.16M_2 - .374P + 1.467Q_2 \quad (24a)$$

The twist is given by

$$\theta_c = M_{TC} r_{cc} / E_A I_c \quad (25)$$

with $E_A = 10,600,000$ lb/in^2
$I_c = 0.2147$ in^4
$r_{cc} = 2.619$ in.

Equation (25) becomes

$$10^6 \theta_c = 1.150\ M_{Tc}$$

with Eq. (24) this gives

$$10^6 \theta_c = - 11.1B - 5.36F_2 + 5.20N - 2.48M_2 - .430P + 1.683Q_2 \quad (27a)$$

The radial deflection of ring 'c' is given by

$$\delta_c = r_{cc} r_{c1} c_N P / E_A A_c - r_{cc} r_{dm} Q_2 / E_a A_c + r_{cc} r_N N(\cos \alpha - \mu \sin \alpha) / E_A A_c \quad (28)$$

with $A_c = 1.368$ in^2 Eq. (28) reduces to,

$$10^6 \delta_c = 0.243P - 0.389Q_2 + 0.160N \quad (29a)$$

we get with $\mu = - 0.6$ for sliding in the opposite direction.

$$M_{Tc} = - 9.65B - 4.66F_2 + .784N - 2.16M_2 - .374P + 1.467Q_2 \quad (24b)$$

giving

$$10^6 \theta_c = - 11.1B - 5.36F_2 + .900N - 2.48M_2 - .430P + 1.683Q_2 \quad (27b)$$

Likewise

$$10^6 \delta_c = 0.243P - 0.389Q_2 + .424N \quad (29b)$$

13.3.6 Interaction of parts of connector

13.3.6.1 Cylinder 'a' and Ring 'b'

We know that for compatibility

$$\delta_a = \delta_b + \theta_b b_c \tag{30}$$

$$\theta_a = \theta_b \tag{31}$$

Using Eqs. (6), (7), (14a) and (16a) we get relations permitting the elimination of M_1 and Q_1 for $\mu = 0.6$ with $b_c = 0.571$ in.

$$-1.289M_1 - 1.061Q_1 + .353P + .0527F_1 = .0771P + .1380Q_1 - .0545N + .571(3.25G + 1.95F_1 - 1.66N + .0937P + .498Q_1 - .873M_1) \tag{32a}$$

$$3.49M_1 + 1.289Q_1 = 3.25G + 1.95F_1 - 1.66N + .0937P + .498Q_1 - .873M_1 \tag{33a}$$

Solving these for M_1 and Q_1 gives

$$M_1 = -.0064P + 1.077G + .637F_1 - .556N \tag{34a}$$

$$Q_1 = +.1533P - 1.828G - 1.057F_1 + .973N \tag{35a}$$

Similarly for $\mu = -0.6$, Eq. (34) and (35) are

$$M_1 = -.0064P + 1.077G + .637F_1 - .0255N \tag{34b}$$

$$Q_1 = +.1533P - 1.828G - 1.057F_1 + .1180N \tag{35b}$$

With Eqs. (14) and (16)

$$10^6\delta_b = .0983P - .252G - .146F_1 + .0797N \tag{36a}$$

$$10^6\delta_b = .0983P - .252G - .146F_1 - .1280N \tag{36b}$$

and

$$10^6\theta_b = .1757P + 1.40G + .86F_1 - .69N \tag{37a}$$

$$10^6\theta_b = .1757P + 1.40G + .86F_1 + .063N \tag{37b}$$

13.3.6.2 Cylinder'd' and Ring 'c'

We know that for compatibility

$$\delta_d = \delta_c - c_c\theta_c$$

$$\theta_d = \theta_c$$

Using Eqs. (8), (9), (27) and (29) we get for $\mu = +.6$

$$7.50M_2 + 4.88Q_2 + 1.365P + .204F_2 = 0.243P - 0.389Q_2$$

$$+0.160N - 0.679(- 11.1B - 5.36F_2 + 5.20N - 2.48M_2 - .430P + 1.683Q_2) \quad (38a)$$

$$24.95M_2 + 7.50Q_2 = - 11.1B - 5.36 F_2 + 5.20N$$

$$-2.48M_2 - .430P + 1.683Q_2 \quad (39a)$$

Solving for M_2 and Q_2 gives

$$M_2 = 0.0146P - .811B - .383F_2 + .373N \quad (40a)$$

$$Q_2 = - .1428P + 1.912B + .882F_2 - .865N \quad (41a)$$

Similarly with $\mu = -.6$ we have

$$M_2 = +0.0146P - .811B - .383F + .048N \quad (40b)$$

$$Q_2 = - .1428P + 1.912B + .882F_2 - .073N \quad (41b)$$

With Eqs. (29) and (41)

$$10^6\delta_c = 0.299P - .744B - .343F_2 + .496N \quad (42a)$$

$$10^6\delta_c = .299P - .744B - .343F_2 + .452N \quad (42b)$$

and

$$10^6\theta_c = - .706P - 5.87B - 2.92F_2 + 2.81N \quad (43a)$$

$$10^6\theta_c = - .706P - 5.87B - 2.92F_2 + .657N \quad (43b)$$

13.3.6.3 Ring 'b' and Ring 'c'

These rings are in contact at the seal circle. The relative axial displacement of one ring centroid with respect to the other is given by

$$\Delta_{bc} = \frac{\delta_b}{\tan\alpha} - \frac{\delta_c}{\tan\alpha} - \frac{r_{tb}\theta_b}{\sin\alpha} + \frac{r_{tc}\theta_c}{\sin\alpha} \quad (44)$$

where Δ_{bc} = is positive for an increase in axial distance from 'b' to 'c'

$\alpha = 37^o$

r_{tb} = distance from centroid of ring 'b' cross-section to normal through contact point = .217 in. (positive towards point of 'b').

r_{tc} = distance from centroid of ring 'c' cross-section to normal through contact point = +.264 in. (positive in same direction as r_{tb}).

with these values Eq. (44) becomes

$$\Delta_{bc} = 1.327\delta_b - 1.327\delta_c - .360\theta_b + .438\theta_c \quad (45)$$

13.3.6.4 Axial Shortening at Bolt

The increase in flange spacing at the bolts is given by

$$\Delta_B = \Delta_{bc} - (r_{c6} - r_{b3})\theta_e - (r_{b3} - r_{bc})\theta_b + (r_{c6} - r_{cc})\theta_c \quad (46)$$

with Eqs. (45), (21), (37), and (43) and

$r_{c6} = 3.106$ in.
$r_{b3} = 2.885$ in.
$r_{bc} = 2.134$ in.
$r_{cc} = 2.619$ in.

we get

$$\Delta_B = 1.327\delta_b - 1.327\delta_c - 1.111\theta_b + .925\theta_c - .221\theta_e \quad (47)$$

Substituting the values in Eqs. (36), (37), (38), (39), and (21) into (47) gives

$$10^6\Delta_B = - 8.88B + 1.934G - 1.150F_1 - 2.24F_2 - 1.114P + 2.82N \quad (48a)$$

$$10^6\Delta_B = - 8.88B + 1.934G - 1.150F_1 - 2.24F_2 - 1.114P - .23N \quad (48b)$$

13.3.7 Interrelation of Forces

From Eq. (1), $G = 1.077B$ (49)

Since the external axial load and bending moment on the connector are zero for the loading conditions considered

$$F_1 = -\pi r_{a1}^2 P/(2\pi r_{am}) \quad (50)$$

with $r_{a1} = 2.010$ in.
$r_{am} = 2.235$ in.

$$F_1 = - 0.905P \quad (51)$$

and

$$F_2 = - \pi r_{d1}^2 P/(2\pi r_{dm}) \quad (52)$$

where $r_{d1} = 2.010$ in.
$r_{dm} = 2.16$ in.

giving, $F_2 = - 0.936P$ (53)

With $\mu = +.6$ Eq. (3) gives

$$N = 1.43B + 1.03F_1 = 1.43B - .93P \quad (54a)$$

with $\mu = - .6$

$$N = 12.6B + 9.1F_1 = 12.6B - 8.2P \quad (54b)$$

13.3.7 Solutions for Different Conditions

13.3.7.1 Initial Tightening

The bolt force for a given torque (see ABMA-STD-18 for 3/8" bolts) used in tightening is given in Ref. 13. For a steel bolt with the friction coefficient taken as 0.15, the bolt force per circumferential inch is B_s = 1650 lb/in. With an 0.10 friction coefficient, B_s = 2360 lb/in. We will use the latter value as typical of lubricated steel. For an aluminum bolt in which the aluminum head bears on steel and the aluminum nut bears on aluminum the bolt force will depend on which end is being tightened. If we tighten the aluminum head bearing on the steel, an effective friction coefficient of 0.6 is about as low as might be expected. With this value B_a = 250 lb/in.

Returning to Eq. (54a) which corresponds to the direction of the contact friction during bolt tightening we get:

$$N_s = 1.43(2360) = 3380 \text{ lb/in} \qquad (55)$$
(steel bolts, no pressure)

$$N_a = 1.43(250) = 358 \text{ lb/in} \qquad (56)$$
(aluminum bolts, no pressure)

The value of Δ_B from Eq. (48a) with Eq. (49) is

$$10^6\Delta_{B1s} = -8.88(2360) + 1.934(1.077)(2360) + 2.82(3380)$$
$$= -6{,}500 \text{ in.} \qquad (57)$$

and

$$10^6\Delta_{B1a} = -8.88(250) + 1.934(1.077)(250) + 2.82(358)$$
$$= -689 \text{ in.} \qquad (58)$$

13.3.7.2 Pressure 1500 psi, Temperature Rise 55°F

With pressure we take the direction of friction at the seal as requiring μ =-0.6, (i.e. the b Eqs.). The bolt force B will change to a value which we will now determine. From Eq. (54b)

$$N = 12.6B - 8.2(1500) = 12.6B - 12{,}300 \qquad (59)$$

From Eq. (48b), (49), (51), (53) and (59) we get the new value of Δ_B in terms of B for a pressure change only

$$10^6\Delta_{B2}(\text{pres}) = -8.88B + 1.934(1.077)B - 1.150(-.905)(1500)$$
$$- 2.24(-.936)(1500) - 1.114(1500) - .23(12.6B - 12{,}300)$$
$$= -9.70B + 5{,}860 \qquad (60)$$

The coefficient of expansion for the steel ring 'b' is 8.7 x 10^{-6}/°F while for the aluminum ring 'c' it is 12.5 x 10^{-6}/°F. Due to the 55°F temperature rise then

$$10^6\delta_b(\text{temp}) = r_{bc}(55)(8.7) = 1020 \tag{61}$$

$$10^6\delta_c(\text{temp}) = r_{cc}(55)(12.5) = 1800 \tag{62}$$

With Eq. (47) and including the effect of axial growth in 'b' and 'c'

$$10^6\Delta_{B2}(\text{temp}) = 1.327(1020 - 1800) + 8.7(55)(.757) + 12.5(55)(1.243)$$
$$= 184 \tag{63}$$

Then combining Eqs. (60) and (63)

$$10^6\Delta_{B2} = - 9.70B + 6{,}000 \tag{64}$$

The increase in flange spacing at the bolts is obtained from Eqs. (64) and (57) in the case of steel bolts.

$$10^6\Delta\Delta_{B2s} = 10^6\Delta_{B2} - 10^6\Delta_{B1s}$$

$$= - 9.70B_{s2} + 6000 + 6500 = - 9.70B_{s2} + 12500 \tag{65}$$

The steel bolt length is increased by the change in bolt force and temperature change. It is thus also given by

$$10^6\Delta\Delta_{B2s} = (B_{s2} - B_{s1})\frac{\ell 10^6}{AE_s} + 8.7(\Delta T)(\ell) \tag{66}$$

where

ℓ = bolt length = 2.00 in.

A = bolt area per inch = 0.0679 in^2/in

ΔT = temperature change = 55^oF

E_s = 28,200,000 lb/in^2

giving

$$10^6\Delta\Delta_{B2s} = (B_{s2} - 2360)(1.044) + 957$$
$$= 1.044B_{s2} - 1508 \tag{67}$$

Combining (65) and (67)

$$B_{s2} = 1300 \text{ lb/in} \tag{68}$$

Similarly using (64) and (58) for aluminum bolts

$$10^6\Delta\Delta_{B2a} = 10^6\Delta_{B2} - 10^6\Delta_{B1a}$$

$$= - 9.70B_{a2} + 6000 + 689 = - 9.70B_{a2} + 6700 \tag{69}$$

The aluminum bolt length is increased to

$$10^6\Delta\Delta_{B2a} = (B_{a2} - B_{a1})\frac{\ell 10^6}{AE_a} + 12.5(\Delta T)(\ell) \tag{70}$$

with

$$E_a = 10,600,000 \text{ lb/in}^2$$

$$10^6 \Delta\Delta_{B2a} = (B_{a2} - 250)(2.785) + 1377$$

$$= 2.785B_{a2} + 680 \qquad (71)$$

Combining (69) and (71)

$$B_{a2} = 480 \text{ lb/in} \qquad (72)$$

From Eqs. (59), (68) and (72)

$$N_{s2} = 4,100 \text{ lb/in} \qquad (73)$$

$$N_{a2} = - 6,200 \text{ lb/in} \qquad (74)$$

(The negative sealing force with aluminum bolts given by Eq. (74) indicates a high probability of leakage. Since the friction coefficients are only estimated values, one cannot be certain).

13.3.7.3 Differential Pressure 1440 psi, Temperature Drop 363°F

We continue to take the direction of friction at the seal as requiring $\mu = - 0.6$, (i.e. the b Eqs.). The bolt force will change to a value which we will now determine. From Eq. (54b)

$$N = 12.6B - 8.2(1440) = 12.6B - 11800 \qquad (75)$$

From Eq. (48b), (49), (51), (53) and (75) we get the new value Δ_B in terms of B for a pressure change only

$$10^6 \Delta_B(\text{pres}) = - 8.88B + 1.934(1.077)B - 1.150(- .905)(1440)$$
$$- 2.24(- .936)(1440) - 1.114(1440) - 0.23(12.6B - 11,800)$$
$$= - 9.70B + 5623 \qquad (76)$$

The new value of Δ_B for a temperature change of - 363°F is found by analogy with Eq.(63) as

$$10^6 \Delta_{B3}(\text{temp}) = - 1220 \qquad (77)$$

Combining (76) and (77)

$$10^6 \Delta_{B3} = - 9.70B + 4400 \qquad (78)$$

The increase in flange spacing at the bolts is obtained from Eqs. (78) and (57) for steel bolts

$$10^6 \Delta\Delta_{B3s} = 10^6 \Delta_{B3} - 10^6 \Delta_{B1s}$$

$$= - 9.70B_{s3} + 4400 + 6500 = - 9.70B_{s3} + 10900 \qquad (79)$$

The steel bolt length is increased by the change in bolt force and temperature change. In analogy with Eq. (67) we get

$$10^6 \Delta\Delta_{B3s} = 1.044 B_{s3} - 8800 \tag{80}$$

Combining Eqs. (80) and (79)

$$B_{s3} = 1850 \text{ lb/in} \tag{81}$$

Similarly using (78) and (58) for aluminum bolts

$$10^6 \Delta\Delta_{B3a} = 10^6 \Delta_{B3} - 10^6 \Delta_{B1a}$$

$$= - 9.70 B_{a3} + 4400 + 689 = - 9.70 B_{a3} + 5100 \tag{82}$$

In analogy with Eq. (71)

$$10^6 \Delta\Delta_{B3a} = 2.785 B_{a3} - 9,800 \tag{83}$$

Combining Eqs. (82) and (83)

$$B_{a3} = 1200 \text{ lb/in} \tag{84}$$

From Eqs. (75), (81) and (84)

$$N_{s3} = + 11,500 \text{ lb/in} \tag{85}$$

$$N_{a3} = + 3,300 \text{ lb/in} \tag{86}$$

It is of considerable interest that the decrease in temperature has resulted in positive sealing pressure with the aluminum bolts whereas in Section 13.3.7.2 it was negative.

13.3.7.4 Differential Pressure 3140 psi, Temperature Drop 363°F

We continue to take the direction of friction as requiring $\mu = - 0.6$. From (54b)

$$N = 12.6B - 8.2(3140) = 12.6B - 25800 \tag{86}$$

Comparable to Eq. (76) we have

$$10^6 \Delta_{B4}(\text{pres}) = - 9.70B + 12260 \tag{87}$$

Combining (77) and (87) since temperature is unchanged

$$10^6 \Delta_{B4} = - 9.70B + 11,000 \tag{88}$$

In analogy with Eq. (79)

$$10^6 \Delta\Delta_{B4s} = - 9.70 B_{s4} + 17,500 \tag{89}$$

Equating (89) and (80)

$$B_{s4} = 2460 \text{ lb/in} \tag{90}$$

Similarly using (88) and (58) for aluminum bolts

$$10^6 \Delta\Delta_{B4a} = - 9.70 B_{a4} + 11,700 \tag{91}$$

Equating (91) and (83)

$$B_{a4} = 1720 \text{ lb/in.} \tag{92}$$

From Eqs. (86), (90) and (92)

$$N_{s4} = 5,200 \text{ lb/in.} \tag{93}$$

$$N_{a4} = - 4,100 \text{ lb/in.} \tag{94}$$

13.3.7.5 Connector Stresses Developed by Loading

From the bolt loads calculated it was found that when steel bolts were used, some yielding of the tip section of ring 'b' could occur due to hoop stresses. This condition was local, however, and did not affect the sealing region.

13.3.8 Leakage Flow

The contact region between ring 'b' and ring 'c' involves a Hertzian loading. The radius of curvature of ring 'c' is 1.83 in. Ring 'b' is considered flat. We then use the theory for a cylinder bearing on a flat surface. From Ref. 15, Eq. (221), the contacting width in an axial direction is given by

$$w_{elas} = 4\sqrt{N(k_b + k_c)R_c} \tag{95}$$

where

$$k_b = \frac{1 - \nu_b^2}{\pi E_b} \; ; \; 10^6 k_b = .0103$$

$$k_c = \frac{1 - \nu_c^2}{\pi E_c} \; ; \; 10^6 k_c = .0273$$

$$R_c = 1.83 \text{ in.}$$

Substituting values in (95) gives

$$w_{elas.} = .00105\sqrt{N} \tag{96}$$

The maximum contacting stress assuming full elasticity is given by Ref. 15, Eq. (225), as

$$\sigma_{elas} = 1210\sqrt{N} \tag{97}$$

With Eqs. (55), (56), (73), (74), (85), (86) we get the values of w_{elas} and σ_{elas} in Table 1 by the use of Eqs. (96) and (97). The values of σ_{eff} are estimated on the basis that they must be less than σ_{elas} and that they never exceed three times the 35,000 psi yield stress of the steel. The value of w_{eff} is obtained by dividing N by σ_{eff}. We assume that the leakage flow between rings 'b' and 'c' will be the same as that through two flat pieces of width w_{eff} pressed together to a stress σ_{eff}. Using the ratio of σ_{eff}/σ_{yp} where σ_{yp} is the yield stress, Fig. 33.9 was entered to obtain h_e/h_r where m=0,

h_e = effective leakage flow path height (microinches)

h_r = effective surface roughness of each surface across the direction of flow = 8 micro-inches

TABLE 1 Hertzian stresses and contact width and estimated equivalent constant contact stress and width including effect of yielding of steel (ring 'b') at 35,000 psi.

Bolt	Loading	N lb/in	σ_{elas} lb/in^2	w_{elas} in	σ_{eff} lb/in^2	w_{eff} in	$\frac{\sigma_{eff}}{\sigma_{yp}}$	$\frac{h_e}{h_r}$
Steel	1	3380	70,500	.061	60,000	.0563	1.71	.83
Aluminum	1	358	22,900	.020	22,900	.0156	.654	1.44
Steel	2	4100	77,700	.067	63,000	.0650	1.80	.78
Aluminum	2	-6200	—	—	—	—	—	—
Steel	3	11500	130,000	.120	87,000	.1320	2.48	.49
Aluminum	3	3300	69,700	.060	58,000	.0570	1.66	.85
Steel	4	5200	87,500	.076	67,000	.0780	1.91	.74
Aluminum	4	-4100	—	—	—	—	—	—

The effective value of h_r may not be the value commonly obtained from a roughness gage. It will depend also on the nature of the machining operations and on the degree of relative interaction of the mating surfaces.

The corresponding flow can be obtained from Fig. 22.1 if we consider the effect of the 60 psi external pressure to be negligible. Entering this figure with the values of h_e in Table 2 we obtain the values of Q_u, the uncorrected flow. The corrected flow, Q is obtained from the relation,

$$Q = Q_u\left(\frac{2\pi r_N}{5}\right)\left(\frac{0.1}{w_{eff}}\right)\left(\frac{459 + 68}{459 + T}\right) \qquad (98)$$

where T is the gas temperature in degrees F. We know that

r_N = 2.02 in.

TABLE 2 Estimated Leakage Flow

Bolt	Loading	Pres lb/in^2	h_e/h_r	h_e microinch	Q_u lb/hr	T ^oF	w_{eff} in	Q lb/hr
steel	1	0	.83	6.6	0	70	.0563	0
alum	1	0	1.44	11.5	0	70	.0156	0
steel	2	1500	.78	6.2	.0009	125	.0650	.0032
alum	2	1500	large	—	—	125	—	large*
steel	3	1440	.49	3.9	.0002	-293	.1320	.0012
alum	3	1440	.85	6.8	.0010	-293	.0570	.014
steel	4	3140	.74	5.9	.0020	-293	.0780	.021
alum	4	3140	large	—	—	-293	—	large*

* NOTE: Relative leakage for cases 2 and 4 of aluminum bolts is not calculable since separation was indicated.

Equation (98) can be written as

$$Q = Q_u(134)/\left[w_{eff}(459 + T)\right] \tag{99}$$

The results show that for steel bolts the leakage flow has a maximum value in the order of 0.02 lb. of helium per hour. In the case of the aluminum bolts there is large leakage at 125^{o}F, 1500 psi and at - 293^{o}F, 3200 psi. At - 293^{o}F and 1500 psi the aluminum bolts give a leakage in the order of 0.01 lb of helium per hour.

13.3.9 Discussion

A major source of uncertainty in the analysis is the correct choice for friction coefficients. This affects both the bolt forces achieved by a given tightening torque and the interaction of mating parts at the point of sealing.

The loadings considered do not include end loads or moments due to interaction between pipe and missile. It seems likely that such forces could increase the leakage.

The large radius of curvature on ring 'c' appears to affect sealing adversely. A smaller radius here should increase the sealing action but might impair re-use because of permanent set in the sealing region.

13.4 References

1. E.O. Waters, D.B. Rossheim, D.B. Wesstrom and F.S.G. Williams, Development of General Formulas for Bolted Flanges, Taylor Forge and Pipe Works, Chicago, Illinois.

2. ASME Boiler and Pressure Vessel Code, Section VIII, "Rules for Construction of Unfired Pressure Vessels", 1959 Edition.

3. E.C. Rodabaugh, Discussion of "Effect of Internal Pressure on Stresses and Strains in Bolted-Flanged Connections", Pressure Vessel and Piping Design, ASME, 1960, p. 131.

4. United Aircraft Products, Inc., Handbook of United Metallic O-rings, Bulletin No. 596191A, Dayton, Ohio, 1959.

5. Huntsville Memo M-P&VE-PE #733.

6. W.M. Dudley, "Deflection of Heat Exchanger Flanged Joints As Affected by Barreling and Warping", Trans. ASME, Nov. 1961, pp. 460-465.

7. Dwg. No. SK20-1297, George C. Marshall Space Flight Center, NASA, Huntsville, Alabama.

8. S. Timoshenko and S. Woinowsky-Krieger, Theory of Plates and Shells, McGraw-Hill Book Co., 1959.

9. S. Timoshenko, Strength of Materials, Part II, D. Van Nostrand Co. 1959.

10. ABMA-STD-18, 7 July 1958, Torque Specifications: Threaded Fasteners.

11. T.F. Durham, R.M. McClintock and R.P. Reed, Cryogenic Materials Data Handbook, U.S. Dept. of Commerce, National Bureau of Standards.

12. S.L. Hoyt (ed), Metals Properties, ASME Handbook, McGraw-Hill, 1954.

13. L.S. Marks (ed.), Mechanical Engineers' Handbook, Fifth Edition, McGraw-Hill 1941.

14. Machine Design Plastics Book, September 20, 1962, Chapter 12.

15. S. Timoshenko, Theory of Elasticity, First Edition, McGraw-Hill, 1934.

DISTRIBUTION LIST FOR REPORTS ON CONTRACT NAS 8-4012

NASA Headquarters, Washington 25, D.C.

Mr. Henry Burlage, Jr.
Chief, Liquid Propulsion Systems, RPL (3)

Mr. A.O. Tischler
Assistant Director for Propulsion, MLP (1)

NASA, Marshall Space Flight Center, Huntsville, Alabama

Mr. Charles Wood (M-P&VE-PT), Technical Manager (24)
Office of Technical Information, M-MS-IPC
Contracting Officer, M-P&C-C
Patent Office, M-PAT

NASA Other Locations

Technical & Scientific Information Facility
Attention: NASA Representative, Code CRT
P.O. Box 5700, Bethesda, Maryland (24)

Attention: Technical Librarian

Ames Research Center
Moffett Field, California (2)

Goddard Space Flight Center
Greenbelt, Maryland (2)

Jet Propulsion Laboratory
California Institute of Technology
4800 Oak Grove Drive
Pasadena, California (2)

Langley Research Center
Langley Field, Virginia (2)

Lewis Research Center
21000 Brookpark Road
Cleveland 35, Ohio (2)

Marshall Space Flight Center
Huntsville, Alabama (2)

Manned Spacecraft Center
Houston, Texas (2)

Advanced Research Projects Agency
Pentagon, Room 3D154
Washington 25, D.C.

Aeronautical Systems Division
Air Force Systems Command
Wright-Patterson Air Force Base, Ohio

Attention: Technical Librarian

Air Force Missile Development Center
Holloman Air Force Base, New Mexico

Air Force Missile Test Center
Patrick Air Force Base, Florida

Air Force Systems Command, Dyna-Soar
Air Force Unit Post Office
Los Angeles 45, California

Army Ordnance Missile Command
Redstone Arsenal, Alabama

Armed Services Technical Information Agency
Arlington Hall Station
Arlington 12, Virginia

Arnold Engineering Development Center
A.E.O.R.
Tullahoma, Tennessee

Bureau of Naval Weapons
Department of the Navy
Washington 25, D.C.

Central Intelligence Agency
2430 E. Street, N.W.
Washington 25, D.C.

Headquarters, United States Air Force
Washington 25, D.C.

Office of Naval Research
Washington 25, D.C.

Attention: Technical Librarian

Picatinny Arsenal
Dover, New Jersey

Rocket Research Laboratories
Edwards Air Force Base, California

U.S. Naval Ordnance Test Station
China Lake, California

U.S. Atomic Energy Commission
Technical Information Services
Box 62
Oak Ridge, Tennessee

Liquid Propellant Information Agency
Johns Hopkins University
Applied Physics Laboratory
8621 Georgia Avenue
Silver Spring, Maryland

Aerojet-General Corporation
P.O. Box 296
Azusa, California

Aerojet-General Corporation
P. O. Box 1947
Sacramento 9, California

Aeronutronic
A Division of Ford Motor Company
Ford Road
Newport Beach, California

Aerospace Corporation
2400 East El Segundo Boulevard
El Segundo, California

Arthur D. Little, Inc.
Acorn Park
Cambridge 40, Massachusetts

Astropower, Inc., Subsidiary of Douglas
Aircraft Company, Inc.
2968 Randolph Avenue
Costa Mesa, California

Astrosystems, Inc.
82 Naylon Avenue
Livingston, New Jersey

Atlantic Research Corporation
Edsall Road and Shirley Highway
Alexandria, Virginia

Attention: Technical Librarian

Beech Aircraft Corporation
Boulder Facility
Box 631
Boulder, Colorado

Bell Aerosystems Company
P. O. Box 1
Buffalo 5, New York

Bendix Systems Division
Bendix Corporation
Ann Arbor, Michigan

Boeing Company
P. O. Box 3707
Seattle 24, Washington

Convair (Astronautics)
Division of General Dynamics Corporation
P. O. Box 2672
San Diego 12, California

Curtiss-Wright Corporation
Wright Aeronautical Division
Wood-ridge, New Jersey

Douglas Aircraft Company, Inc.
Missile and Space Systems Division
3000 Ocean Park Boulevard
Santa Monica, California

Fairchild Stratos Corporation
Aircraft Missiles Division
Hagerstown, Maryland

General Electric Company
Missile and Space Vehicle Department
Box 8555
Philadelphia, Pennsylvania

General Electric Company
Rocket Propulsion Units
Building 300
Cincinnati 15, Ohio

Grumman Aircraft Engineering Corporation
Bethpage, Long Island, New York

Kidde Aero-Space Division
Walter Kidde and Company, Inc.
675 Main Street
Belleville 9, New Jersey

Attention: Technical Librarian

Lockheed Aircraft Corporation
Missile and Space Division
Sunnyvale, California

Lockheed Propulsion Company
P.O. Box 111
Redlands, California

Marquardt Corporation
16555 Saticoy Street
Box 2013 - South Annex
Van Nuys, California

Martin Division
Martin Marietta Corporation
Baltimore 3, Maryland

Martin Denver Division
Martin Marietta Corporation
Denver, Colorado

McDonnell Aircraft Corporation
P. O. Box 6101
Lambert Field, Missouri

North American Aviation, Inc.
Space & Information Systems Division
Downey, California

Northrup Corporation
1001 East Broadway
Hawthorne, California

Pratt & Whitney Aircraft Corporation
Florida Research & Development Center
West Palm Beach, Florida

Radio Corporation of America
Astro-Electronics Division
Defense Electronic Products
Princeton, New Jersey

Reaction Motors Division
Thiokol Chemical Corporation
Denville, New Jersey

Republic Aviation Corporation
Farmingdale
Long Island, New York

Attention: Technical Librarian

Rocketdyne (Library Dept. 586-306)
Division of North American Aviation, Inc.
6633 Canoga Avenue
Canoga Park, California

Space General Corporation
9200 Flair Avenue
El Monte, California

Space Technology Laboratories
P. O. Box 95001
Airport Station
Los Angeles 45, California

Stanford Research Institute
333 Ravenswood Avenue
Menlo Park, California

TAPCO Division
Thompson-Ramo-Wooldridge, Inc.
23555 Euclid Avenue
Cleveland 17, Ohio

Thiokol Chemical Corporation
Redstone Division
Huntsville, Alabama

United Aircraft Corporation
East Hartford Plant
400 Main Street
Hartford, Connecticut

United Technology Corporation
587 Methilda Avenue
Sunnyvale, California

Vought Astronautics
Box 5907
Dallas 22, Texas

Armour Research Foundation
Illinois Institute of Technology
10 West 35th Street
Chicago 16, Illinois

Battelle Memorial Institute
505 King Avenue
Columbus 1, Ohio

National Bureau of Standards
Cryogenic Engineering Laboratory
Boulder, Colorado